CoMFA and CoMSIA Investigations Revealing Novel Insights into the Binding Modes of Dopamine D3 Receptor Agonists

Frank Boeckler, Ursula Ohnmacht, Thomas Lehmann, Wolfgang Utz, Harald Hübner, and Peter Gmeiner*

Department of Medicinal Chemistry, Emil Fischer Center, Friedrich-Alexander University, Schuhstrasse 19, D-91052 Erlangen, Germany

Received September 7, 2004

As an extension of a series of dopamine D_3 receptor agonists involving FAUC 54, ex-chiral pool synthesis, and biological evaluation of 3-substituted 7-aminotetrahydroindolizines was performed. Considering the structural features of both series of enantiomers, we developed a novel alignment hypothesis for D_3 agonists, allowing for the placement of the aromatic moieties on two alternative, adjacent positions. CoMFA and CoMSIA analyses yielded significant cross-validated q^2 values of 0.726 and 0.590, respectively, when a newly invented program application (IRAS) controlling the alignment selection proved to be useful. Employing the CoMFA/CoMSIA contribution maps, we were able to transform a previously constructed homology model of the D_3 receptor from an inactive into an activate state. Besides the established ionic interactions, we propose π-stacking with Phe6.51 and a hydrogen bond between His6.55 and the acyl moiety to be primarily involved in the D_3 receptor binding of FAUC 54 and its analogues.

Introduction

Since the D_3 receptor was cloned from a cDNA library by Sokoloff and co-workers[1] in 1990, considerable progress has been made toward understanding its physiological function and pharmacological impact. As a member of the D_2-like subfamily of dopamine receptors, D_3 is coupled negatively to adenylyl cyclase. Strong evidence exists for a preferential postsynaptic location, but also some subsets are found presynaptically, when controlling dopamine synthesis and release and neuronal firing.[2] Being preferentially expressed in brain regions associated with emotional and cognitive functions, the D_3 receptor affects behavioral properties, such as locomotor activity, reinforcement, and reward, and, thus, has been regarded as an interesting therapeutic target for the treatment of schizophrenia,[3] Parkinson's disease,[4] drug-induced dyskinesia,[5] and cocaine addiction.[6] Additionally, D_3 seems to be involved in cortical development during gestation, obviously orchestrating neuronal migration and differentiation.[7]

Starting from both isomers of enantiopure asparagine, we have recently reported an ex-chiral pool synthesis of 7-dipropylaminotetrahydroindolizines (ATHI) mimicking structural features of both lysergic acid and the D_3 agonist (*R*)-7-OH-DPAT when the (*S*)-3-formyl derivative FAUC 54 displayed preferential D_3 agonist properties with nanomolar binding affinity.[8] Extending the pioneering work of Wilcox and co-workers[9−11] and further QSAR studies on D_2 ligands[12−17] as well as D_3 and D_4 antagonists,[16,18−21] we herein present an extended SAR investigation on a series of chiral 7-aminotetrahydroindolizines (ATHIs), gaining insights into the structural requirements for D3 agonists. Employing a training set of 34 ATHIs and 10 commercially available dopaminergics, significant CoMFA and CoMSIA models for the design of D_3 agonists could be obtained (Scheme 1). Since the carbaldehyde function in position 3 of the heterocyclic scaffold proved to be beneficial for D_3 receptor recognition, we tried to extend our recently described set of ATHIs **(*S*)-1**−**9** and **(*R*)-1**−**9**[8] by the 3-substituted target compounds **10**−**17** and **28**−**30**, which should be synthesized by application of a previously established ex-chiral pool approach.

Scheme 1

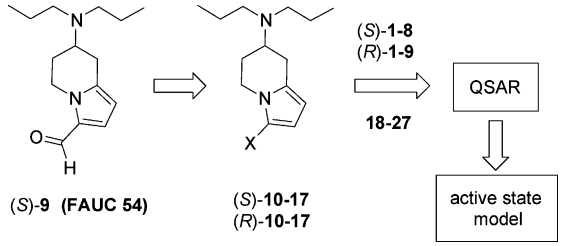

Results and Discussion

Taking advantage of our recently described ex-chiral pool protocol for the synthesis of enantiomerically pure tetrahydroindolizines from asparagine, the central building blocks **(*S*)-1**[22] and **(*S*)-9** (FAUC 54)[8] could be prepared in sufficient quantity for further functionalization. Thus, regioselective Friedel−Crafts acylation of **(*S*)-1** led to the 3-acetyl, 3-benzoyl, 3-trifluoroacetyl, and 3-trichloroacetyl derivatives **(*S*)-11**, **(*S*)-12**, **(*S*)-13**, and **(*S*)-14**, respectively (Scheme 2). Transformation of the trichloroacetyl functionality of **(*S*)-14** into an ethyl carboxylate group could be realized upon treatment with sodium ethoxide. When compared to the 3-formyl derivative **(*S*)-9** (FAUC 54), which displayed a favored *s*-trans structure, the sterically more demanding carbon substituents X make an *s*-cis conformation even more unlikely.

* To whom correspondence should be addressed. Phone: +49(9131)-8529383. Fax: +49(9131)8522585. E-mail: gmeiner@pharmazie.uni-erlangen.de.

10.1021/jm049269+ CCC: $30.25
Published on Web 03/01/2005

Scheme 2

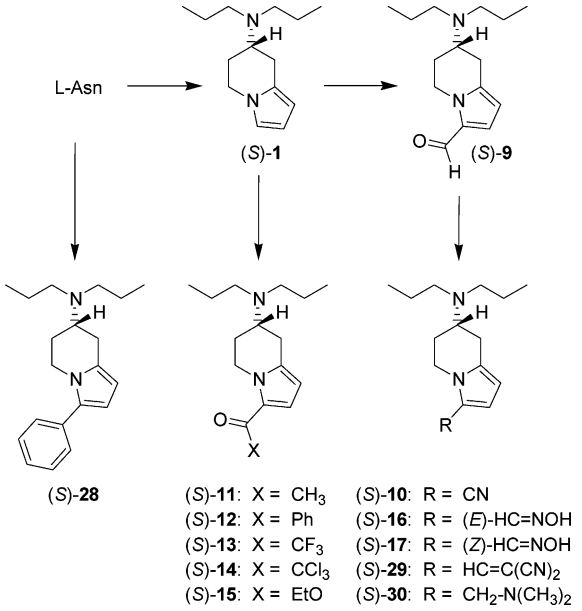

As a complement to the formal exchange of the formyl hydrogen position, the sp^2 formyl oxygen should be also displaced, giving access to putatively *s*-cis-substituted derivatives. Thus, treatment of **(*S*)-9** with malonodinitrile under Knoevenagel conditions led to the dicyanovinyl derivative **(*S*)-29**. On the other hand, oxime formation gave a mixture of the π-diastereomers **(*S*)-16** and **(*S*)-17**, which could be readily separated by flash chromatography. According to diagnostic NOEs, the (*E*)-isomer **(*S*)-16** displayed *s*-trans geometry, whereas the (*Z*)-isomer diastereomer **(*S*)-17** unambiguously showed the *s*-cis conformation, which is obviously due to steric interactions between the HO-group and position 4 of the ring system, preventing the *s*-trans conformation.

Further structural variations involved the transformation of the formyl sp^2 carbon into an sp system, which could be performed by oxime formation and subsequent dehydration, giving access to the carbonitrile **(*S*)-10**. Reductive amination of the carbaldehyde group furnished the dimethylaminomethyl derivative **(*S*)-30** with a sp^3 C-substituent. Finally, the enlargement of the π-system of the formyl group should be investigated. Thus, the 3-phenylindolizine **(*S*)-28** was approached from *(S)*-4-amino-2-dibenzylaminobutan-1-ol,[22] which is readily available from natural asparagine. The reaction sequence involved the Paal−Knorr reaction with 4-oxo-4-phenylbutanal, cationic cyclization after activation of the primary alcohol with help of Tf_2O, and exchange of the benzyl protecting group by propyl substituents, which was done by hydrogenolysis and subsequent reductive propylation. Synthesis of the series of (*R*)-ATHIs was done analogously, when starting from (*R*)-asparagine.

Except for the moderate D_3 ligands **12**, **14**, and **15**, the binding data of the newly synthesized ATHIs clearly indicated that the (*S*)-enantiomers showed substantially higher affinity. The formal exchange of the formyl hydrogen of **(*S*)-9** (FAUC 54)[8] by carbon substituents resulted in only weak reduction of D_3 binding. Enlargement of the substituents, however, caused a more substantial decrease. For the (*S*)-enantiomers of the oximes **16** and **17**, the *E*-configuration, obviously resulting in an *s*-trans conformation (according to NMR experiments), resulted in an improved D_3 receptor recognition, which is in agreement with the *s*-trans form of the lead compound **(*S*)-9** in its bioactive conformation. Whereas the 3-phenyl-ATHI **28** and the dimethylaminomethyl derivative **30** gave poor binding, the (*S*)-enantiomer of the dicyanovinyl derivative **29** showed an acceptable pK_i of 7.22. Formal exchange of the formyl functionality by a cyano group proceeded under retention of D_3 recognition, as indicated by a pK_i of 8.14 for the carbonitrile **(*S*)-10**. A comparison of the subtype selectivity and the ligand efficacy of **(*S*)-10** with the

Table 1. Dopamine Receptor Binding Data and Intrinsic Activity of FAUC 54 ((*S*)-9) and (*S*)-10 Compared to the Reference Compounds Pramipexole and Quinpirole

		FAUC 54 ((*S*)-9)	(*S*)-10	pramipexole (**25**)	quinpirole (**27**)
			K_i Values ± SEM (nM)[a]		
bD_1	K_i low	>20000	>20000	>20000	>20000
hD_{2long}	K_i high	52 ± 13	190 ± 38	21 ± 4.9	63 ± 17
	K_i low	6900 ± 1800	6500 ± 1700	6300 ± 1300	3100 ± 800
hD_{2short}	K_i high	41 ± 7.0	130 ± 59	21 ± 5.1	35 ± 6.0
	K_i low	3000 ± 170	5100 ± 1300	1900 ± 560	3000 ± 590
hD_3	K_i high	5.3 ± 1.1	7.2 ± 3.2	0.88 ± 0.15	24 ± 6.3
	K_i low	150 ± 16	140 ± 29	38 ± 7.0	420 ± 140
$hD_{4.4}$	K_i high	32 ± 8.5	40 ± 18	8.1 ± 1.1	1.8 ± 0.093
	K_i low	2500 ± 220	9700 ± 2800	130 ± 22	53 ± 5.9
			Incorporation of [^{3}H]Thymidine		
rD_{2long}	EC_{50}[b]	11	42	9.2	4.8
	intrinsic activity[c]	98	99	85	100
rD_{2short}	EC_{50}	79	130	12	17
	intrinsic activity	101	95	103	100
hD_3	EC_{50}	1.1	2.4	1.5	2.6
	intrinsic activity	86	59	93	100
$hD_{4.2}$	EC_{50}	4200		15	8.7
	intrinsic activity	67	0	84	100

[a] K_i values in nM ± SEM are based on the means of 2−10 experiments each done in triplicate. [b] EC_{50} values are derived from the mean curves of 2−8 experiments and are in units of nM. [c] Rate of incorporation of [^{3}H]thymidine (%) as evidence for mitogenetic activity relative to the maximal effect of the full agonist quinpirole (=100%).

Chart 1. 7-Aminotetrahydroindolizine (ATHI) Derivatives **1**−**17** and Literature D_3 Agonists **18**−**27** Used in the Training Set

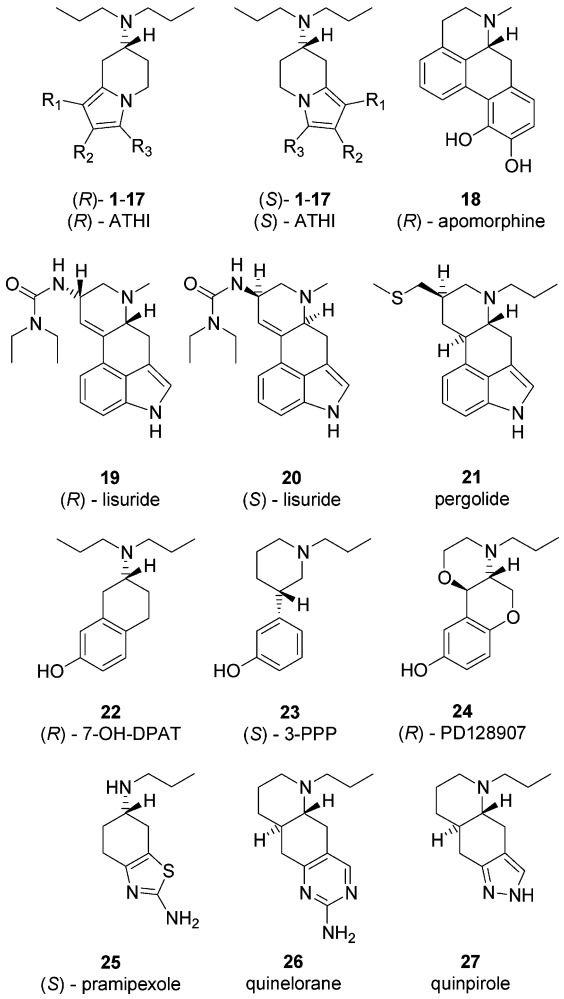

dopamine receptor binding and efficacy profiles of **(*S*)-9**[8] and the well-established dopaminergics pramipexole (**25**) and quinpirole (**27**) clearly indicated D_3 preference and significantly better K_i values for the high-affinity binding site, except for quinpirole favoring the D_4 subtype (Table 1). Interestingly, the ED_{50} values for ligand efficacy monitored by a mitogenesis assay sometimes do not correlate very well with the K_i high concentrations, which might be due to different agonist-directed trafficking. For the D_3 subtype, ED_{50}/K_i ratios between 0.1 and 1.7 were calculated. Except for the D_4 subtype, the data of the functional assay clearly corroborate the agonist properties deduced from the biphasic competition curves.

Predictive Power—CoMFA and CoMSIA. Using our properly selected training set of 44 D_3 ligands (Chart 1 and Table 2), involving literature compounds with extended structural diversity, we obtained statistically significant QSAR models (Table 3). The initial PLS analysis of the CoMFA model (A) without applying a σ_{min} data filter yielded a cross-validated q^2 of 0.726 with five components used, while the analogous PLS analysis of the CoMSIA model (F) gave a cross-validated q^2 of 0.590 using four components. Increasing the minimum level of field variation σ_{min} to purpose an efficient reduction of noise, the CoMFA model differed slightly around the initial value, giving a cross-validated q^2 of

Table 2. Data Set of 44 Compounds Used in the Training Set and Eight Compounds Used as Test Set To Predict Binding Affinities[a]

compound				pK_i-	ΔpK_i	
no.	R_1	R_2	R_3	(exp)	CoMFA	CoMSIA
			Training Set			
(*R*)-1	H	H	H	5.78	0.054	0.040
(*S*)-1	H	H	H	6.24	−0.239	−0.466
(*R*)-2	CH_3	H	H	5.84	0.219	−0.226
(*S*)-2	CH_3	H	H	6.17	0.101	0.068
(*R*)-3	H	CH_3	H	6.04	−0.155	0.220
(*S*)-3	H	CH_3	H	6.10	0.072	−0.111
(*R*)-4	H	H	CH_3	6.21	0.082	0.206
(*S*)-4	H	H	CH_3	6.38	−0.318	−0.231
(*R*)-5	CH_2OH	H	H	6.49	0.200	0.582
(*S*)-5	CH_2OH	H	H	5.01	−0.244	0.120
(*R*)-6	H	CH_2OH	H	5.85	0.244	0.007
(*S*)-6	H	CH_2OH	H	5.07	−0.105	−0.169
(*R*)-7	H	H	CH_2OH	6.14	−0.030	0.312
(*S*)-7	H	H	CH_2OH	6.38	−0.167	−0.116
(*R*)-8	CHO	H	H	6.30	−0.232	−0.046
(*S*)-8	CHO	H	H	5.44	−0.339	0.149
(*R*)-9	H	H	CHO	5.74	0.060	−0.320
(*S*)-9	H	H	CHO	8.28	0.083	0.885
(*R*)-10	H	H	CN	5.55	0.090	−0.204
(*S*)-10	H	H	CN	8.14	0.256	0.285
(*R*)-11	H	H	CH_3CO	5.55	0.176	−0.190
(*S*)-11	H	H	CH_3CO	7.34	−0.158	0.463
(*R*)-12	H	H	PhCO	5.81	0.104	−0.030
(*S*)-12	H	H	PhCO	5.72	0.051	−0.310
(*R*)-13	H	H	CF_3CO	5.60	−0.069	−0.474
(*S*)-13	H	H	CF_3CO	7.64	−0.039	0.340
(*R*)-14	H	H	CCl_3CO	7.06[b]	0.028	0.429
(*S*)-14	H	H	CCl_3CO	6.58	−0.243	0.375
(*R*)-15	H	H	EtOCO	6.49[b]	0.001	0.374
(*S*)-15	H	H	EtOCO	5.36	0.067	−1.435
(*R*)-16	H	H	*E*-HCNOH	5.68	0.098	0.155
(*S*)-16	H	H	*E*-HCNOH	7.51	0.023	−0.340
(*R*)-17	H	H	*Z*-HCNOH	5.32	0.041	−0.288
(*S*)-17	H	H	*Z*-HCNOH	7.31[b]	0.112	−0.099
18		(*R*)-apomorphine		7.23	−0.127	−0.030
19		(*R*)-lisuride[c]		9.85	0.142	−0.195
20		(*S*)-lisuride[d]		8.46	0.021	0.161
21		pergolide		9.07	−0.196	−0.167
22		(*R*)-7-OH-DPAT		9.10	0.507	0.274
23		(*S*)-3-PPP		7.60	0.001	−0.131
24		(*R*)-PD128907		8.85	−0.114	−0.207
25		(*S*)-pramipexole		9.14	0.015	0.519
26		quinelorane		9.03	−0.119	−0.121
27		quinpirole		7.62	0.097	−0.007
			Test Set[e]			
(*R*)-28	H	H	Ph	5.62	0.039	−0.388
(*S*)-28	H	H	Ph	5.10	−1.082	−1.518
(*R*)-29	H	H	$HCC(CN)_2$	5.22	0.079	−0.635
(*S*)-29	H	H	$HCC(CN)_2$	7.22	0.538	0.304
(*R*)-30	H	H	$CH_2N(CH_3)_2$	4.92	−0.561	−0.174
(*S*)-30	H	H	$CH_2N(CH_3)_2$	5.44	−0.103	−0.156
(*R*)-31[f]	(*R*)-*N*-formyltetrahydroindole			7.36	0.353	1.247
(*S*)-31[f]	(*S*)-*N*-formyltetrahydroindole			7.41	−0.494	0.296
R^2_{pred}[g]					0.817	0.607

[a] The experimental binding affinities toward the dopamine D_3 receptor are expressed as pK_i (−log K_i) values. The K_i is given in nM and based on the means of 2−10 experiments each done in triplicate (for SEM and more details, please see TableS1 in the Supporting Information). ΔpK_i is the error of fitted (training set) or predicted (testset) binding affinities and is defined as ($pK_{i,experimental}$ − $pK_{i,fitted/predicted}$). [b] K_i values are determined from a combined competition curve consisting of all normalized data points from several individual experiments. [c] (+)-(5*R*,8*S*)-lisuride. [d] (−)-(5*S*,8*R*)-lisuride. [e] Deviations reflect the prediction for the Rff-aligned compounds. [f] EPC synthesis of **(*R*)-** and **(*S*)-31** was done by treatment of (*R*)- and (*S*)-5-*N*,*N*-dipropylamino-4,5,6,7-tetrahydroindole[53] with n-BuLi (2 euiv) at −78 °C for 5 min, subsequent addition of ethyl formate (2 equiv) and warming up to 0 °C. [g] Predicted r^2 calculated with a standard deviation (SD) obtained from the test set only: 0.807 (CoMFA) and 0.586 (CoMSIA).

Table 3. Summary of the Results from Different PLS Runs of the CoMFA and CoMSIA Analyses

	CoMFA					CoMSIA				
reg. focus.	no	no	no	0.2[a]	0.3[a]	no	no	no	0.3[a]	0.4[a]
σ_{min}	**0.0**	1.0	5.0	0.5	0.5	**0.0**	1.0	5.0	0.5	0.5
PLS run	A	B	C	D	E	F	G	H	I	J
q^2_{cv}	**0.726**	0.711	0.741	0.746	0.763	**0.590**	0.588	0.556	0.626	0.646
s_{PRESS}	**0.719**	0.739	0.699	0.692	0.677	**0.868**	0.871	0.905	0.840	0.828
r^2	**0.983**	0.982	0.979	0.986	0.986	**0.918**	0.919	0.905	0.946	0.954
S	**0.180**	0.186	0.199	0.164	0.160	**0.387**	0.386	0.419	0.318	0.300
F	**433.1**	406.6	356.2	525.0	552.9	**109.7**	110.7	92.5	134.3	126.6
components	**5**	5	5	5	6	**4**	4	4	5	6
descriptors	**19308**	2827	733	2270	1841	**49500**	6499	1727	3839	3038
fraction										
steric	**0.745**	0.663	0.567	0.650	0.630	**0.036**	0.045	0.076	0.104	0.128
electrost	**0.255**	0.337	0.433	0.350	0.370	**0.181**	0.188	0.214	0.189	0.185
hydroph						**0.254**	0.247	0.243	0.218	0.202
donor						**0.327**	0.319	0.281	0.300	0.294
acceptor						**0.202**	0.201	0.186	0.189	0.190

[a] Appended exponent field controlling the sharpness of the focusing.

0.711 (five components) at $\sigma_{min} = 1.0$ kcal·mol^{-1} (B) and 0.741 (five components) at $\sigma_{min} = 5.0$ kcal·mol^{-1} (C). Applying the same data filtering levels on the CoMSIA model yielded identical or slightly impaired cross-validated q^2 values of 0.588 (four components) and 0.556 (four components) at $\sigma_{min} = 1.0$[23] (G) and 5.0[23] (H), respectively. Using region focusing as an advanced method of noise reduction together with a standard data filter of $\sigma_{min} = 0.5$, the model quality was slightly improved for the CoMFA model to a q^2 of 0.746 (five components) at a focusing exponent of 0.2 (D) and to 0.763 (six components) at a focusing exponent of 0.3 (E). Similar small enhancements were obtained for the CoMSIA model using focusing exponents of 0.3 (I: $q^2_{cv} = 0.626$, five components) and 0.4 (J: $q^2_{cv} = 0.646$, six components). However, it should be noted that, frequently, an increase of q^2_{cv} values by less than 5% for the use of an additional component is considered inappropriate due to the "parsimony-principle".[24] Interestingly, while the noise reduction in the CoMFA model decreased the fraction of the steric contribution from 74.5% down to 56.7%, it was increased by the noise reduction in the CoMSIA model from 3.6% up to 12.8%. The other CoMSIA field types typically contribute to the full model in the order donor (28.1−32.7%) > hydrophobic (20.2−25.4%) > acceptor (18.6−20.2%) ≈ electrostatic (18.1−21.4%).

In contrast to CoMSIA, CoMFA analyses give a noticeable dependence of q^2 values on the relative placement of the aligned ligands with respect to the probe grid.[25] Thus, to test our CoMFA model for robustness, we applied a modified Aps procedure, originally published by Wang et al.,[26] which systematically translates the aligned dataset in space, followed by a SAMPLS analysis after each displacement. The histogram plot of the resulting 1000 model variants showed to be approximately corresponding to a normal distribution of the obtained q^2 values (Figure 1). The quite narrow range of the values between 0.656 and 0.746 with 50% of the values lying between 0.701 and 0.721 indicated that our initial CoMFA model is comparably stable. Considering that almost all superior model variants were based on one or more additional components, we decided to retain our initial model for further analysis and interpretation of the fields.

The predictive power of the CoMFA (PLS mode A) and CoMSIA (PLS mode F) analysis was further examined

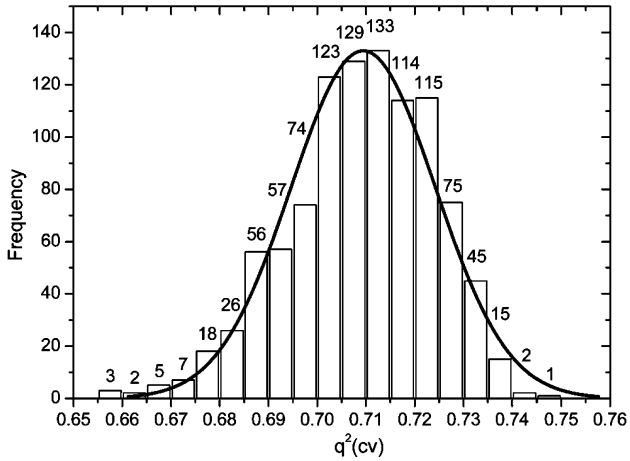

Figure 1. Histogram showing the distribution of the q^2_{cv} values calculated as SAMPLS[54] leave-one-out cross-validation after systematic translation of the aligned molecules within the lattice by the APS (all placement search) script of Wang et al.[26] The stepwise displacement of all ligands in steps of 0.1 Å along the *x*-, *y*-, and *z*-axis yields 1000 models. Their q^2_{cv} values are shown binned into 19 histogram ranges of 0.005 units size. The numbers on top of each corresponding bar indicate how many models lie in the respective q^2 range. For comparison, a fitted normal distribution curve is overlaid on the histogram bars.

using a test set of eight compounds (**(*R*)-/(*S*)-28**−**31**, Chart 2) that had been omitted from the training set. Due to our model building procedure, two alignments had to be regarded for each ligand, the Tsar-based and the rigid field fit-based. Although our iterative restriction of alignment strategy IRAS successfully helped to determine for which ligand of the training set realignment with Rff improved the model quality, no general, q^2-independent rule for the alignment preference of the ligands could be derived afterward. Thus, we calculated the predictive r^2 for the pure Tsar and Rff alignments according to the definition of Cramer et al.,[27] giving better results for Rff in both the CoMFA ($r^2_{pred} = 0.817$) and the CoMSIA model ($r^2_{pred} = 0.607$). In addition, we assessed a mean predictive r^2 on basis of the mean predicted pK_i for each ligand. As this approach accounts for both predictions with equal weights, we deem it to yield the most unbiased value. For the external dataset, the CoMFA and CoMSIA model have proven their predictive power, yielding mean r^2_{pred} of 0.652 and 0.573,

Chart 2. 7-Aminotetrahydroindolizine (ATHI) Derivatives **28**−**30** and *N*-Formylaminotetrahydroindole **31** Used in the Test Set

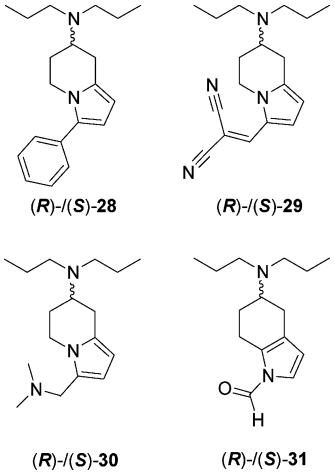

respectively. The corresponding plots of the fitted or predicted versus the experimental binding affinity are shown for the training set (unfilled circles) and the test set (filled circles) in Figure 2. For the test set, the predictions for the Rff-aligned compounds are depicted.

Graphical Interpretation of the Fields. The three-dimensional representations of the CoMFA and CoMSIA field contributions as "stdev*coeff" contour plots reveal where variability in molecules' fields is able to explain experimental binding differences. In the following figures, these plots are exemplified by ligands of high and low affinity. In several directions the aligned ligands were found to be surrounded by yellow contours, indicating that steric interaction with these regions reduce the ligand affinity. Regions 1 and 2, as labeled in Figure 3, strongly delimit the sideward relocatability. Likewise, region 3, which is lying above the partially saturated ring system, and region 4, which is located parallel to the plane of the aromatic moieties, restrict the spatial orientation of the ligands. In contrast, the green contours 5 and 6, which are directly adjacent to the sides of the aromatic moieties, indicate that steric bulk is favorable there. In terms of the substitution pattern at the aromatic part of the tetrahydroindolizines, this generally means that, for the typical orientation of the (*S*)-series ligands, substituents in position 2 are less tolerated than in position 1 or 3, where small substituents are sterically favorable. However, especially in position 3, huge substituents are likely to occupy the surrounding forbidden regions 1, 3, or 4. For the typical orientation of the (*R*)-series, smaller substituents in position 2 are favorable, while any substituent in position 1 collides with the forbidden region 3. For example, the potent ligand **(*S*)-10** (colored orange) places its 3-cyano substituent in the favorable region 5 without any undesirable contacts to regions 1, 3, or 4, while the low potency of **(*R*)-2** can be partly explained as it occupies the unfavorable yellow region 3 with its 1-methyl substituent.

Enclosing the aromatic moieties, a broad blue contour (3 and 4) distinguishes areas where positively charged groups of the ligands enhance binding. It is only disrupted by two red regions (1 and 2), which indicate favorable interactions for negatively charged compound moieties. These regions (1 and 2) correspond to the

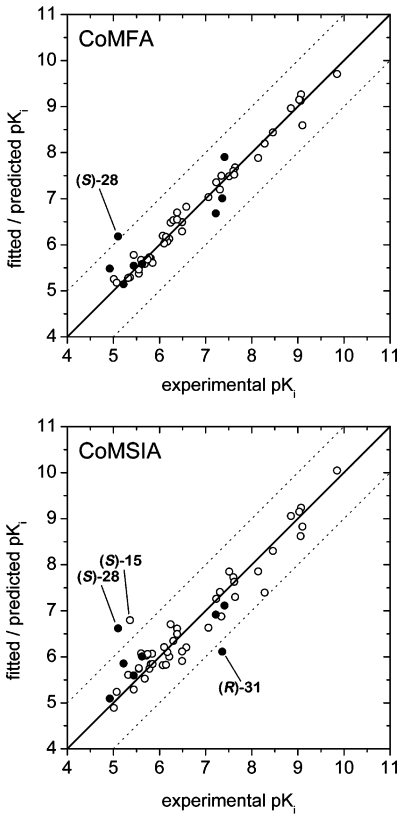

Figure 2. Fitted predictions versus experimental binding affinities for the 44 compounds in the training set (open circles) and the test set (filled circles). In addition to the line of ideal correlation, dotted lines are given, which indicate deviations from the actual pK_i by ±1 logarithmic unit. Outliers are labeled by their compound numbers.

placement of the formyl or acyl groups of several tetrahydroindolizine derivatives, such as for the highly potent **(*S*)-9** (orange), which shows ideal orientation of its 3-formyl oxygen into the red region 1, accounting for strong favorable interactions. In contrast, the electron-rich nitrogen of the 3-cyano group in **(*R*)-10** is falsely placed in a predominantly blue contoured region 3 with only few contacts with the red region 2. The extension of the blue region 3 can be primarily regarded as a result of diverse amino and hydroxyl functions in the highly potent literature compounds **18**−**27**,which are placed with their electron-deficient hydrogens directing to this area.

Although comparison of the results reveals marked similarities between CoMFA and CoMSIA analyses, also a certain amount of complementary information can be found. This has to be seen against the background of the different approaches to obtain the interactions fields. In CoMFA, steric and electrostatic interaction energies are calculated for each molecule at the intersections of a grid embedding that molecule.[27] In contrast, steric, electrostatic, hydrophobic, and hydrogen-bond-donor and -acceptor similarities are described in CoMSIA using Gaussian functions.[28,29] This approach avoids particularly steep potentials next to the molecular surfaces and, thus, determines similarity indices close to the atoms, too. Hence, CoMSIA contour plots denote areas within the ligands that favor or disfavor particular properties, while in CoMFA contour plots areas are distinguished, where the ligand would interact with a

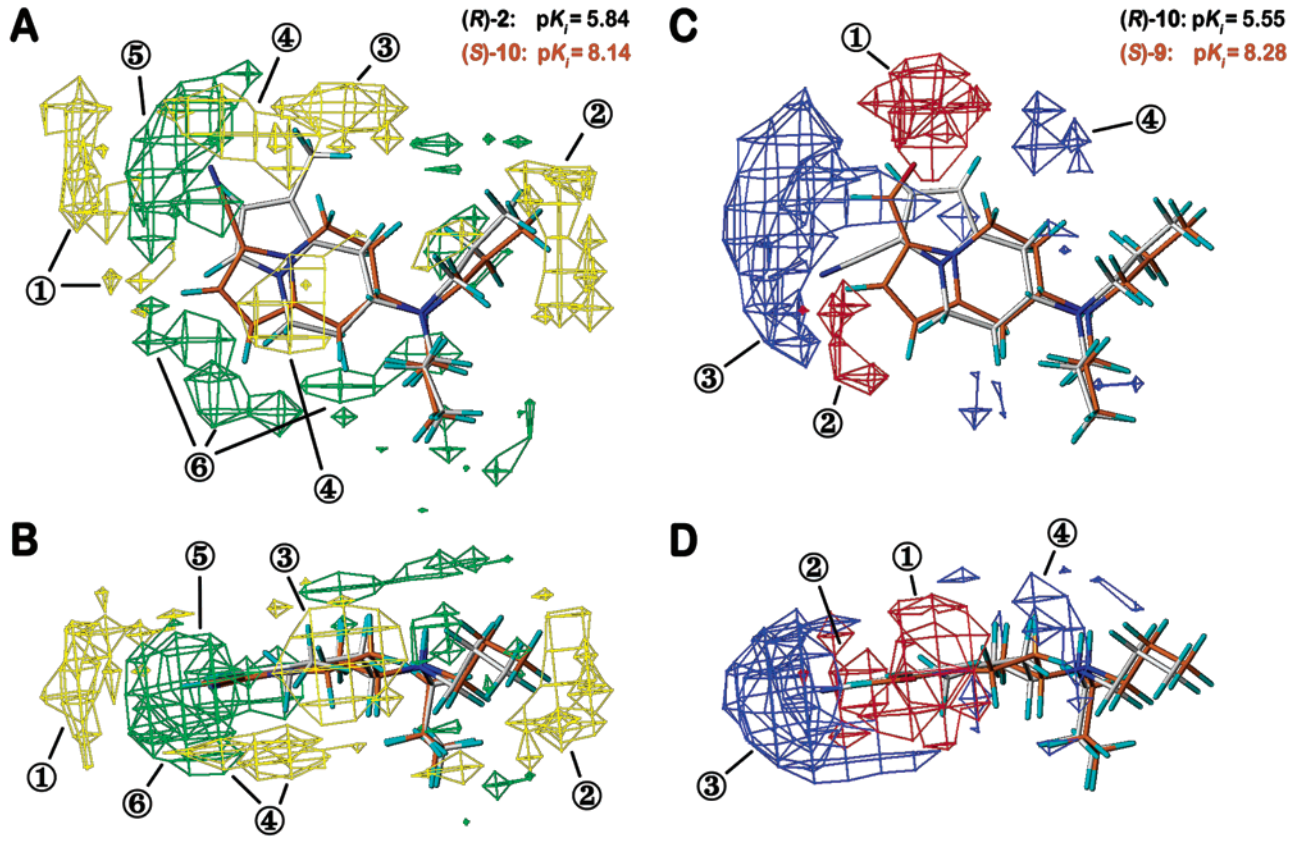

Figure 3. Stdev*coeff contour plots illustrating steric (A + B) and electrostatic features (C + D) as obtained by the final CoMFA analysis. In A + B, regions where steric bulk will enhance affinity are shown enclosed by green contours (contribution level[55] 75%), whereas regions that should be kept unoccupied to prevent decrease of affinity are contoured in yellow (25%). This is exemplified by the high-affinity ligand **(*S*)-10** (orange), which properly occupies the favorable green regions (5 + 6), while the weakly binding ligand **(*R*)-2** (white) shows conflicts with yellow, unfavorable regions (3 + 4). In C + D, red contours (contribution level[55] 20%) encompass regions where electron-rich fragments with negative partial charges will improve affinity. Blue contours (80%) indicate regions where reduced electron density (positive partial charges) is predicted to increase affinity. This is exemplified by the high-affinity ligand FAUC 54 (**(*S*)-9**, orange), for which the preferential conformation of the formyl substituent places the carbonyl oxygen directing to a red area (1) and the formyl hydrogen directing to a blue area (3). The weakly binding ligand **(*R*)-10** (white), in contrast, directs with its electron-rich cyano substituent to the blue region (3), affecting its receptor binding adversely. Depictions A and C are rotated by 90° toward the beholder to give depictions B and D, respectively.

putative environment.[25] CoMSIA contribution plots are typically found to be more contiguous. As a conclusion, exploiting the results of both approaches leads to an optimal interpretation at the 3D level of the QSAR.[30]

Having a closer look at the steric contributions (Figure 4, A), the green isocontour 1, located below the molecules, shows similarity to the green contour 6 in the CoMFA, indicating that the core of the structures should be preferentially placed there and, thus, tends to favor the (*S*)- over the (*R*)-series of the ATHIs. The voluminous green isopleth 2, which is only present in CoMSIA, is primarily caused by the 3,3-diethylureido side chain of the superpotent agonist lisuride (**19**). Additionally, **19** occupies the green isocontour 1 and avoids any contacts with the sterically forbidden yellow regions 3 and 4. These regions 3 and 4 are found to be in accordance with regions 1 and 2 in the CoMFA. The yellow isopleth 3 can be attributed to the low affinities of some ATHIs with very bulky substituents in position 3, such as **(*R*)-/(*S*)-12** or **(*S*)-15**. The isopleth 4 can be explained by the fact that various potent literature agonists (**18**, **23**, **24**, **26**, **27**) have a rigidized ring system instead of a second propyl side chain or completely lack a second propyl side chain at the amine-like pramipexole (**25**) and, thus, do not occupy this region. Exemplifying this findings, the weakly binding ligand **(*R*)-12** places its benzoyl substituent in region3 and its second propyl side chain in region 4, while only partially occupying region 1.

In the electrostatic CoMSIA plots (Figure 4B), only the red isocontour 2 and the leftmost part of isocontour 4 correspond to the red CoMFA isocontours 1 and 2, respectively. The blue isopleth 1, which is located at the π^1-moiety (see Experimental Section—Alignment) and adjacent to it, where the 3-acyl substituents of the ATHIs are typically placed, denotes a region of preferential electron deficiency. Above and below this extended blue region, the red isopleths 2 and 3 indicate areas where electron-rich fragments should be placed. Enclosing the π^2-moiety, the red isopleth 4 reflects the increased potency of several (*S*)-ATHIs compared to their (*R*)-enantiomers (**9**−**11**, **13**, **16**, **17**). While the (*S*)-ATHIs are occupying this π^2-position with their electron-rich aromatic moiety, the (*R*)-ATHIs are unfavorably occupying the blue isopleth 1 at the π^1-position with it. This is exemplified by the structure **(*S*)-9**, which fills out region 4 with its electronegative field, while only partially touching region 1. In addition, its formyl oxygen shows a perfect overlap with region 2, simultaneously placing the positively charged formyl hydrogen

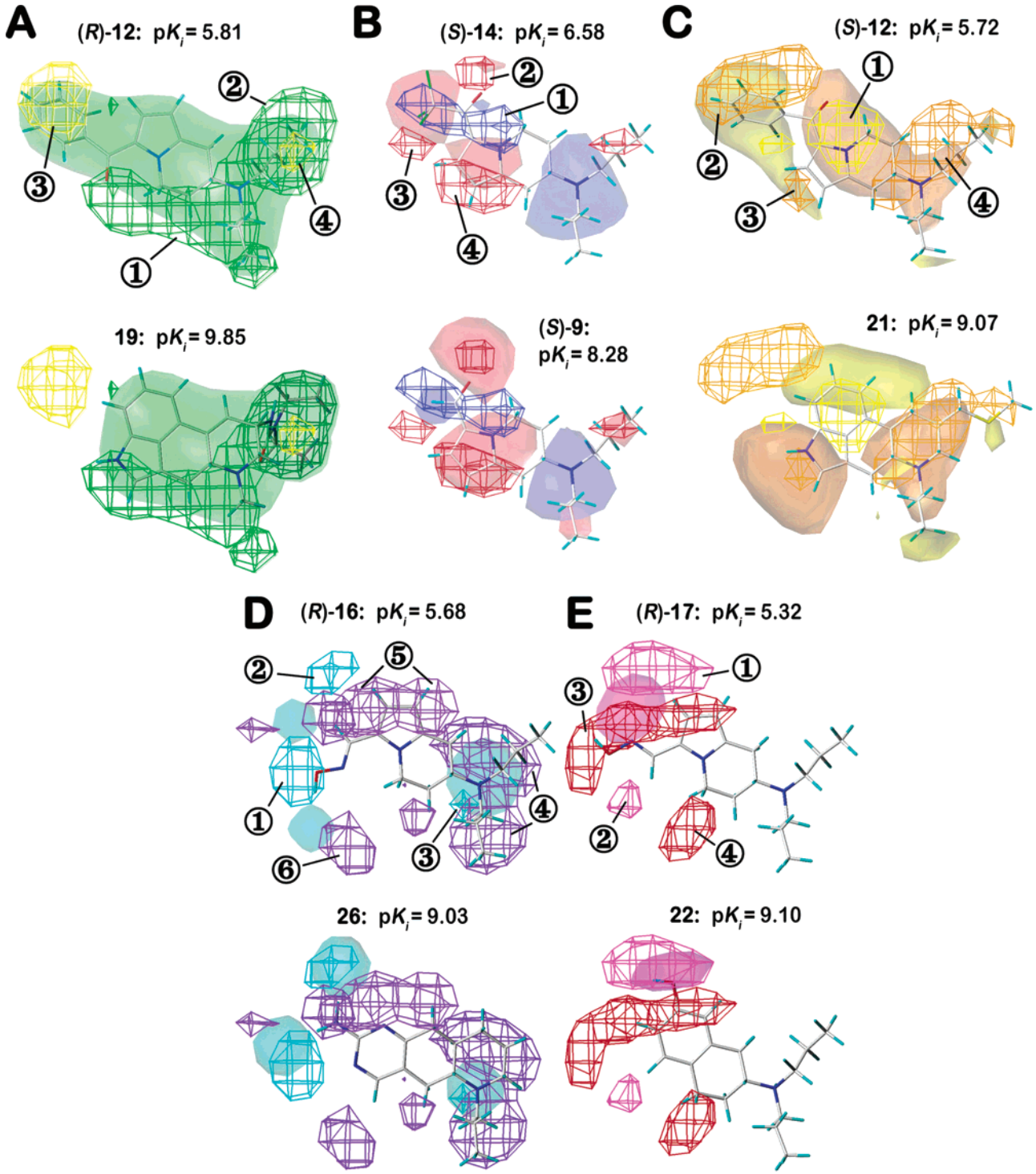

Figure 4. Stdev*coeff contour plots illustrating steric (A), electrostatic (B), hydrophobic (C), hydrogen-bond-donor (D) and -acceptor (E) properties revealed by the final CoMSIA analysis. (A) Green and yellow isopleths (contribution level[55] 80%/20%) indicate regions where steric bulk exerts favorable and unfavorable effects on ligand affinity, respectively. (B) Red and blue isopleths (20%/80%) encompass regions where the affinity is enhanced by an increase of negative and positive charge, respectively. (C) Yellow and orange isopleths (contribution level[55] 80%/20%) enclose regions favorable for hydrophobic and hydrophilic groups, respectively. In D, cyan isopleths (contribution level[55] 80%) indicate regions where a proton acceptor on the receptor site is expected and, thus, hydrogen-bond donors in the ligand directing to these regions are favorable, while donors directing to purple isopleths (10%) are regarded as unfavorable. In E, magenta isopleths (80%) encompass regions where a hydrogen-bond donor on the receptor site is expected and, thus, proton acceptors in the ligand directing to these regions increase the affinity, while proton acceptors in the ligand directing to red regions (20%) decrease the affinity. For all features (A−E), a strongly and a weakly binding ligand are shown in comparison. The steric field (contoured in A at a contribution level of 50%) of the particular ligand is depicted as a transparent green surface, while the positively (85%) and negatively (15%) charged electrostatic fields are shown in B as blue and red transparent surfaces, respectively. The hydrophobic (85%) and hydrophilic (15%) molecular fields (C) are given as transparent yellow and orange surfaces, respectively. In D, the ligand's donor field (70%) is depicted as a transparent cyan surface, while the acceptor field (80%) in E is shown in magenta.

in the blue region 1. In the less potent **(*S*)-14**, the trichloromethyl group obviously withdraws much electron density from the carbonyl moiety and to some extent also from the aromatic ring, leaving the red regions 2 and 4 almost unoccupied, while the electron rich trichloromethyl is adversely oriented toward the blue region 1.

In Figure 4C, orange and yellow contours highlight areas where hydrophilic and hydrophobic properties are preferred, respectively. The yellow isopleth 1 encloses the center of the π-systems, as some rather potent compounds (**18**, **19**, **21**−**24**, **26**, **27**) have lipophilic fields in this area. Various polar amino and hydroxyl functions in ligands with enhanced binding affinity ((***S*)-16**, **(*S*)-17**, **18**, **22**−**26**) are responsible for the large orange isopleth 2, while the small isopleth 3 is mostly determined by heteroaromatic nitrogens in the ligands **19**, **21**, **26**, or **27**. Another orange isocontour (4) is located at and above the protonated amine and is primarily originated from corresponding hydrophilic fields in **19** and **21**−**27**. For example, the less potent **(*S*)-12** exhibits one lipophilic field beside the aromatic moiety and around the phenyl group of the benzoyl substituent and one hydrophilic field around the carbonyl, the heteroaromatic nitrogen, and the protonated amine. As the lipophilic field unfavorably penetrates the orange regions 2 and 3 and the hydrophilic field falsely occupies the yellow region 1, whereas it only partially overlaps the orange field 4, the impaired affinity can be explained. In contrast, the hydrophilic and hydrophobic fields of the highly potent ligand **21** agree quite well with the required contribution maps in region 1, 3, and 4.

The cyan isocontours 1 and 2 besides the aromatic ring in Figure 4D denote regions where proton acceptors are expected in the receptor, and thus, a hydrogen-bond-donating substituent should direct to these regions, whereas they should not direct to the adjacent purple regions 5 and 6. Surrounded on the distant site of the ligands by the purple isocontour 4, the small cyan isocontour 3 reveals the protonated amine as a ubiquitous hydrogen-bond donor that in every ligand needs to be strictly oriented to its Asp3.32 counterpart in the receptor. Displacement of the protonated amine, for example due to bulky substituents at the aromatic system, results in an attenuation of this hydrogen-bond interaction and, hence, to a loss of the ligand affinity. For example, the weakly binding **(*R*)-16** shows a displaced donor field at the protonated amine, reaching into the disallowed region 4, while not even fully including the favorable region 3. Additionally, both putative hydroxyl orientations of the hydroxyiminomethyl substituent do not fit any of the preferential regions 1 or 2. In contrast, the amino function of quinelorane (**26**) directs simultaneously to both regions 1 and 2 and also places its donor field of the protonated amine almost exclusively in the favorable region 3, while only sparsely touching the forbidden region 4.

In the contour plot for the hydrogen-bond-acceptor properties (Figure 4E), two areas (1 and 2) highlighted in magenta represent regions where hydrogen-bond donors are expected on the receptor site. Therefore, placement of acceptor functions of the ligands directing to these magenta isopleths is correlated with enhanced receptor binding, whereas acceptor functions directing to one of the red isopleths (3 or 4) implicate decrease of affinity. These findings are illustrated by the weakly binding **(*R*)-17**, for which the acceptor field of its oxime nitrogen shows only marginal intersection with the favorable magenta isopleth 1 but overlap with the unfavorable red region 3. Contrarily, the acceptor field of the potent agonist 7-OH-DPAT (**22**) exhibits a perfect fit to the magenta isopleth 1, which allows for a partial explanation of the ligand's high affinity.

Modeling of the Corresponding D_3 Binding Site. Modeling the active state of G protein-coupled receptors still is an unsolved challenge, due to the limited experimental data available to date.[31] To gain at least a schematic model of the agonist bound active state of the D_3 receptor binding site, we tried to exploit our CoMFA and CoMSIA fields, representing the binding specific properties of a diverse set of D_3 agonists. Utilizing this structural information, the binding site of our refined D_3 homology model, which meets several characteristics typically ascribed to the inactive state, should be transformed into an activated conformation.[32] For this purpose, the transmembrane helices 6 and 7 (TM6/TM7) were rotated 30°∠45° around their individual helical axes in the direction of TM5, and their orientation in terms of the interhelical angles toward the other helices was slightly adjusted afterward. In addition, some adaptations within the side chain torsions of residues located in the binding site had to be made. Performing these modifications, we were able to derive a model of the binding site in the active state of the D_3 receptor closely matching the CoMFA and CoMSIA information (Figure 5).

An overlay of the steric CoMFA field with the receptor model A reveals that the yellow forbidden isopleths 1 and 2, which delimit the sideward extension of the compounds, correspond to the serine residues in position 5.42 and 5.46 on one side and an aromatic interface between TM3 and TM7 formed by Tyr7.43 and Phe3.28 on the opposite side. The yellow isopleth 3 above the molecules is occupied by His6.55 in the receptor, which is obstructing the ligand's passage to the extracellular medium. In consequence of the rotation of TM6 around its helical axis, PHE6.51 is positioned parallel to the expanded aromatic system of the ligands, allowing for putative π-stacking interactions. This placement of PHE6.51 explains the forbidden yellow region 4, because ligands occupying this region clash with this residue or, when displacing it, necessarily impair the favorable $\pi-\pi$-interactions. The green CoMFA isopleths 5 and 6, indeed, are found to be unoccupied on the receptor site. Only the hydroxyl function of Ser5.42 and an associated water molecule next to SER5.46, which is inserted due to the hydrogen-bonding CoMSIA fields discussed below, are placed in region 5 and 6. However, Ser5.42 easily opens up the required space for region 5 by changing to another χ_1-rotameric state. Likewise, the water associated with Ser5.46 will be displaced without difficulty, if required by a bulky substituent. The other side of the green isopleth 6 is defined by Cys3.36, which also defines the bottom of the binding pocket.

An identical overlay of the electrostatic CoMFA fields with the receptor model B elucidates that the red

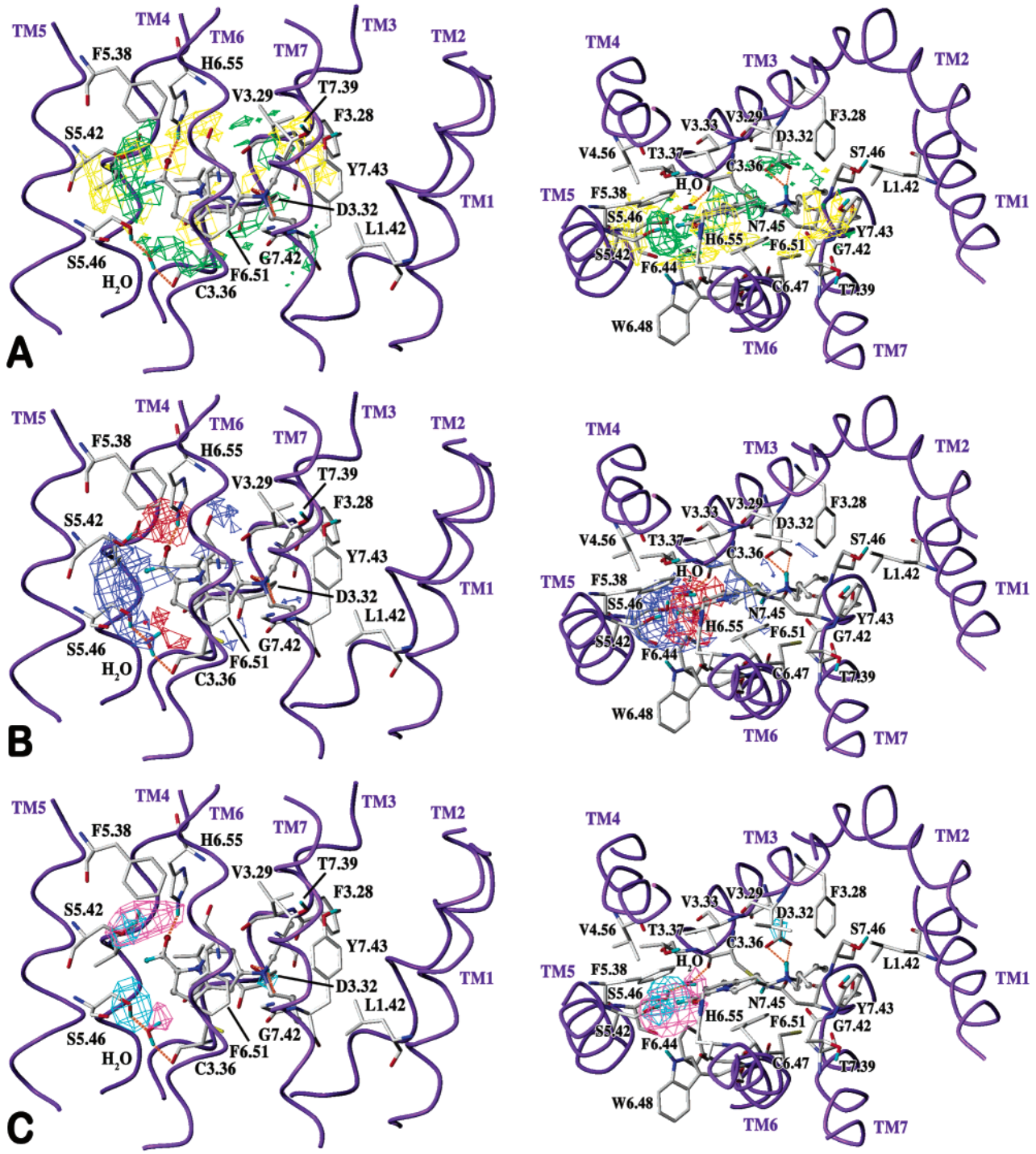

Figure 5. Modified receptor structure overlaid with the steric (A) and electrostatic (B) CoMFA, as well as the hydrogen-bond donor and acceptor CoMSIA contribution plot (C). Upper depictions show the receptor from within the membrane plane, and lower depictions show a perspective from the extracellular medium onto the receptor. Contribution plot contours are presented in agreement with previous figures. Only the section of the receptor containing the binding site and those residues that are directly interacting with the ligands are displayed. The residues are numbered according to the Ballesteros−Weinstein scheme.[40]

isopleths 1 and 2, which indicate preference for electron-rich fragments of the ligand, are determined by the hydrogen attached to the ϵ-nitrogen of His6.55 and the hydrogen of the Ser5.42 hydroxyl group. The orientation of the oxygens in the hydroxyl group of Ser5.42 and Ser5.46 is found to be accountable for the large blue isopleth 3.

Superimposing the CoMSIA hydrogen-bond-donor and -acceptor fields with the receptor model C discloses good agreement with the findings for the electrostatic CoMFA field. The larger magenta isopleth 1 complies with the proton-donating effects of His6.55 and Ser5.42, while the small magenta isopleth 2 is consistent with an associated water molecule fixed between Ser5.46 and Cys3.36. Additionally, the proton acceptor features of the oxygens in Ser5.42 and Ser5.46 account for the cyan isopleths 1 and 2. The small cyan isopleth 3 perfectly fits to the position of Asp3.32.

Conclusion

On the basis of our recently reported potent D_3 ligand **(*S*)-9** (FAUC 54), extended SAR investigations of 34 7-aminotetrahydroindolizines and 10 classical dopaminergics are presented. Considering the structural features of both series of enantiomers, we developed a novel alignment hypothesis for D_3 agonists, allowing for the placement of the aromatic moiety on two alternative, adjacent positions. CoMFA and CoMSIA analyses were performed, yielding significant cross-validated q^2 values of 0.726 and 0.590, respectively, when our newly invented program application IRAS proved to be useful to determine compounds, for which the alignment could be improved using the rigid field fit method. Using a test set of eight compounds, we evaluated the predictive performance of the models on "external ligands", demonstrating their applicability by a mean predictive r^2 of 0.652 for the CoMFA and 0.573 for the CoMSIA model. Applying appropriate adaptations to transform the binding site of a D_3 homology model into an agonist-bound active state, we obtained highly complementary regions between the receptor and our CoMFA/CoMSIA contour maps. This achievement provided the opportunity to interpret our QSAR investigations in terms of real ligand−receptor interactions and to infer the corresponding binding mode postulations. The most relevant findings are outlined in the conceptual Figure 6. All ligands form a reinforced ionic bond between their protonated amine (cyan sphere) and Asp3.32 in the receptor and are anchored with at least one alkyl side chain (yellow cones) in a primarily hydrophobic cavity. The binding site crevice is delimited on one side by serine residues in TM5 and on the other side by an aromatic interface between TM3 and TM7 formed by Phe3.28 and Tyr7.43. The cavity bottom is defined by Cys3.36, while the passage from the cavity to the extracellular medium is obstructed by His6.55. Parallel to the aromatic system of the ligands, Phe6.51 borders the binding pocket and provides favorable π-stacking interactions, while on the opposite side the cavity is restricted by Val3.33. In our model, the ligands are tightly embedded by primarily hydrophobic residues, except for Ser5.42, Ser5.46, and His6.55, which are able to form various hydrogen-bonding interactions. Therefore, under ideal conditions, substituents at the different aromatic moieties can occupy up to two donor (cyan spheres) and two acceptor (magenta spheres) positions. With respect to **(*S*)-9**, the ligand gains affinity by accepting a hydrogen bond, donated by His6.55, with its formyl substituent. As a final conclusion, the combination of CoMFA and CoMSIA as purely ligand-based methods with structure-based homology modeling is capable of both enhancing the interpretability of the QSAR data and contributing to the construction of activated GPCR binding site models.

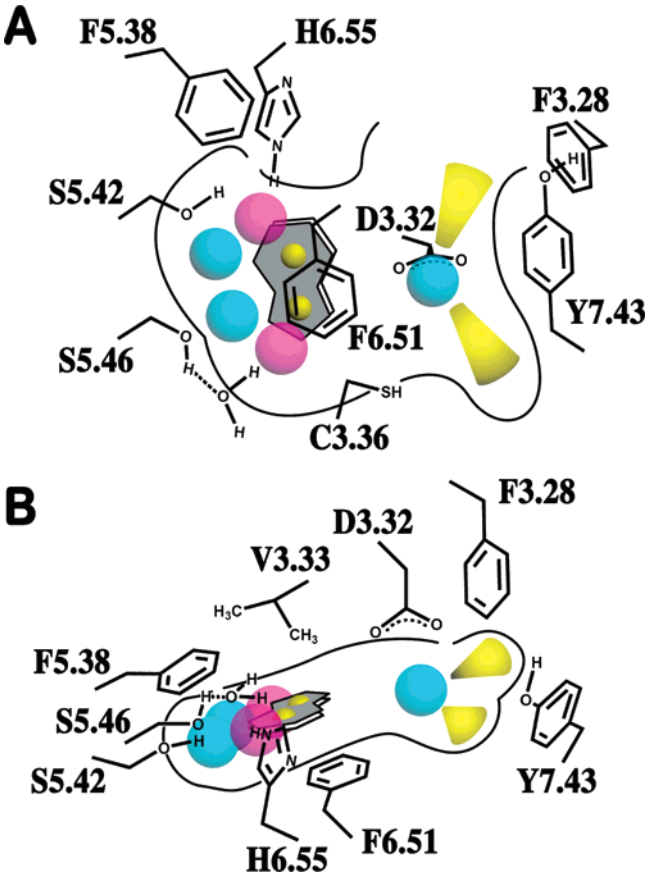

Figure 6. Conceptual illustration of the D_3 receptor agonist binding site, viewed from the membrane plane (A) and from the extracellular medium (B). The extended aromatic system is represented by the abstract indene symbol inferred from the indole partial-structure of the template pergolide. Two yellow spheres within the schematic indene indicate the alternative placement possibilities of a single aromatic system in the ligand. Cyan and magenta spheres denote areas where hydrogen-bond donors and acceptors should be located on the ligand site, respectively. The single cyan sphere next to Asp3.32 marks the protonated amine, which is required to be found in each agonist. Two yellow cones proximate to this cyan sphere represent the hydrophobic side chains.

Experimental Section

Structure Generation and Conformational Analysis. Molecular Modeling and QSAR investigations were performed using primarily Sybyl6.7/6.9[33] and Tsar3.2[34] on Silicon Graphics Indigo2 and Octane2 workstations. A training set of 44 D_3 ligands complemented by a test set of eight ligands was used for all CoMFA and CoMSIA analyses (Charts 1 and 2, Table 1). Under physiological conditions, all of these ligands are expected to be protonated at the tertiary amine function and, hence, all were modeled in this protonated state. The tetrahydroindolizine core structure **(*R*)-1** and all literature compounds were generated using the Sybyl fragment library and initially minimized by applying the standard TRIPOS force field[35] with Gasteiger−Hückel charges.[36] Subsequently, these 11 structures were subjected to an extensive random torsional search (energy cutoff, 10.0 kcal·mol^{-1}; rms threshold, 0.2 Å; max hits, 8; max iterations, 5000; chirality check; extracyclic and nonterminal bonds were defined as rotatable) in order to explore their conformational space efficiently. Using hierarchical cluster analysis, the obtained conformations were classified into five distinct families for every ligand. The lowest energy structure from each of these families, enriched by the 10 most favorable structures of all remaining conformers regardless of their family affiliation, were selected for subsequent semiempirical refinement. The AM1 Hamiltonian within Vamp[37] was employed to optimize all 15 conformations of each ligand, allowing selection among the resulting, suitable structures based upon their calculated heats of formation (ΔH_f). As we can presume that the propyl side chain, which is attached to the protonated amine in almost all the ligands, is most likely interacting with the same part of the binding pocket, all conformations were checked for a common low-energy rotameric state of this propyl side chain. Thus, conformers with a gauche τ_1 (torsion around the N−C bond), a fully staggered τ_2 (torsion around the following C−C bond), and the most

Scheme 3. NMR-Based Evidence for the Preference of the *s*-Trans Isomer in FAUC 54 and Synthetic Strategy To Stabilize the Bioactive Conformation in **11**−**17**

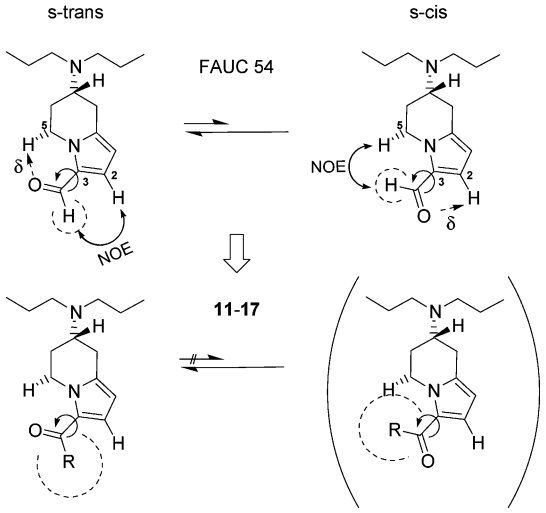

favorable ΔH_f were chosen. Due to its application as an alignment template, pergolide (**21**) was further structurally refined by ab initio calculations. Following preminimization with HF/3-21G*, the molecule was optimized on a B3LYP/6-311G* level of density functional theory.

After the optimized structure of **(*R*)-1** was inverted to yield its (*S*)-enantiomer, we generated the various substituted ATHIs (**2**−**17** and **28**−**30**) by modifying the particular unsubstituted enantiomer, utilizing again the Sybyl fragment library to build the functional groups. Holding the already AM1-optimized core structure rigid as an aggregate within Sybyl, the conformational space of the substituents was sampled with Grid or random torsional searches. NMR investigations on **(*S*)-9** (FAUC 54) have revealed strong NOE between the formyl hydrogen and the pyrrole hydrogen in position 2, as well as substantial downfield shifts (0.7 ppm) of the equatorial hydrogen in position 5, caused by the anisotropy of the carbonyl moiety (Scheme 3). Corresponding to these findings, the *s*-trans isomer is favored by a difference in ΔH_f of more than 5 kcal·mol^{-1}. Considering that this *s*-trans preference also affects the bioactive conformation of **(*S*)-9**,[8] the analogues **11**−**17** were designed to exclude the occupation of the *s*-cis state completely by causing intense steric intramolecular clashes. Thus, in all searches this torsional degree of freedom was restricted from the first. Again, the best 10 structures were subjected to AM1 optimizations in VAMP, which allowed us to distinguish between several low-energy conformers based on ΔH_f.

For quinpirole (**27**), the 1*H*/2*H*-tautomerism in the pyrazole ring has decisive influence on the putative electrostatic and H-bond interaction pattern. Therefore, we calculated the energy difference between both tautomers on successive ab initio levels of theory. The 1.56 kcal·mol^{-1} energy gap found in favor of the 2*H*-form in a HF/6-31G(d) calculation was almost identical (1.59 kcal·mol^{-1}) when enhancing the basis set to 6-311G(d,p). Using second-order Møller−Plesset perturbation (MP2/6-311G(d,p)), the gap further increased to 2.47 kcal·mol^{-1}. Finally, we considered solvation effects by applying a self-consistent reaction field (SCRF) based on the isodensity polarized continuum model (IPCM) upon a HF/6-31+G(d,p) calculation. Again, the gap was enhanced, indicating with a more favorable energy of 6.86 kcal·mol^{-1} the undoubted preference of the 2*H*-tautomer.

Alignment. Finding a suitable alignment is probably the most crucial step to establish a 3D-QSAR model successfully. For D_2 and D_3 receptor agonists a "classical" alignment hypothesis (A_1) has been proposed[38,39] that requires the aromatic moiety of each ligand to be superimposed on one center (π), as well as the protonated amine to be consistently positioned and oriented (Scheme 4). For our dataset, only the latter postulation is actually applicable, as the protonated amine is expected to be interacting with the conserved Asp in position 3.32 in all aminergic receptors.[40] Thus, the N−H-bond should be directing to an identical point in space for all ligands, demonstrating the ability to form a "reinforced ionic bond". The "classical" alignment has been used primarily with agonists showing a stereochemistry that corresponds to the (*S*)-ATHI series, such as the literature compounds apomorphine (**18**), pramipexole (**25**), quinelorane (**26**), and quinpirole (**27**), whereas it cannot produce similarly suitable superpositions for compounds corresponding to the (*R*)-series, like 7-OH-DPAT (**22**), 3-PPP (**23**), or PD128907 (**24**). We obtained significantly better alignments by switching from a single aromatic center π to two alternative aromatic centers, π^1 and π^2 (A_2). The idea for this alignment principle was derived from the substantial binding affinities of (*R*)-lisuride (**19**) and pergolide (**21**), which demonstrate that the receptor easily tolerates placement of aromatic moieties in position π^1, π^2, or even both. Furthermore, the areas of hydrogen-bond interactions (indicated by blue double-headed arrows in Scheme 4) are shifted from π^2 to π^1 in A_2. On the basis of this novel hypothesis, we generated an initial alignment, using a simple rmsd-minimizing atom-fit procedure of the atoms indicated. Choosing **24** and **(*S*)-9** as representative members of the training set, the A_2 alignment on **21** is depicted in Figure 7.

In principle, a third theoretical alignment is conceivable by orienting both enantiomers identically, despite their opposite stereochemistry (B). Consequently, the orientation similarity of the protonated amine and the superposition of the cyclic tetrahydroindolizine structure cannot be optimal at the same

Scheme 4[a]. Classical (A_1), Novel (A_2), and Inverted (B) Alignment Hypotheses

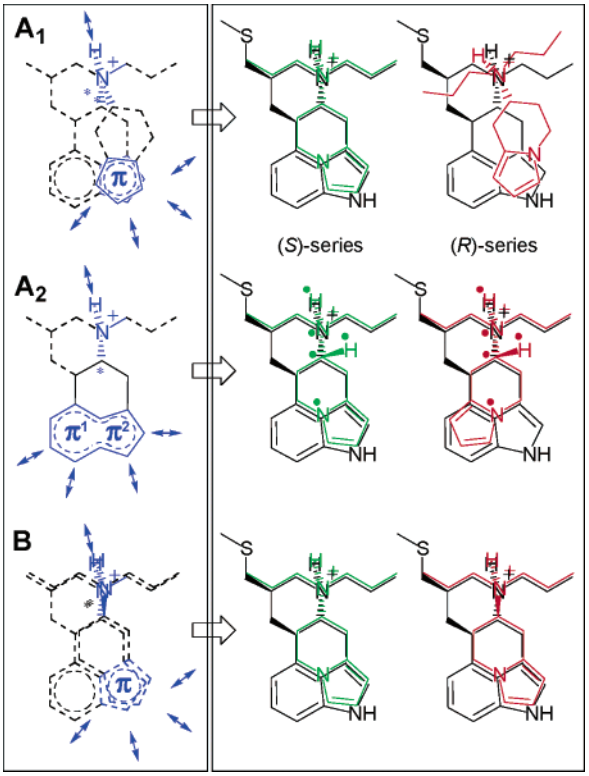

[a] The classical alignment (A_1), which is typically used for (*S*)-series-like molecules, postulates one common aromatic system (π) with several H-bond donors and acceptors attached to it (putative positions indicated by blue double-headed arrows). The novel alignment (A_2) allows superimposition of the aromatic moieties on two alternative aromatic systems ((*R*)-like molecules on π^1 and (*S*)-like molecules on π^2). The five green and red dots in the middle depictions indicate atoms used to generate an initial simple atom fit alignment based on hypothesis A_2. Additionally, a third, theoretical alignment (B) can be defined by orienting both enantiomers identically.

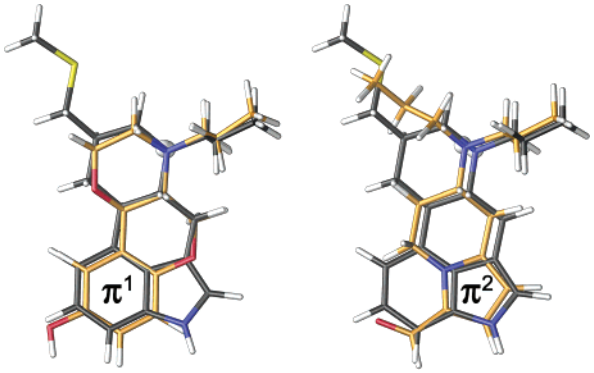

Figure 7. Overlay of PD128907 (**24**) and FAUC 54 ((*S*)-**9**) on pergolide (**21**) shown in their final IRAS alignment. (*S*)-**9** and **24** are aligned on alternative aromatic moieties (π^1 and π^2) of **21** but share the placement of the carbonyl and hydroxyl oxygen, respectively. The hydrogens attached to the protonated amine, which are supposed to interact with Asp3.32 in the receptor, are marked by spherical representations to point out their identical orientation.

time. Following this alternative model to generate an initial alignment, no significant CoMFA model ($q^2 < 0.5$) was found when applying the same procedure as described herein for the favored alignment A_2. Thus, we abandoned the alternative alignment hypothesis B.

To refine this coarse alignment involving molecular similarity aspects, it was used as an input for the Tsar[34]-module Asp,[41] which enabled us to perform an alignment by comparison of steric overlap and molecular electrostatic potentials. First, Vespa charges[42] were calculated for all molecules using the semiempirical program package Vamp. These atom-centered partial charges, which are obtained by a fit of the electronic wave function to the atomic positions, have the advantage that the anisotropy of the electron distribution around the molecule, in particular for aromatic systems, is described very well.

To quantify the relative orientation of two molecules, a combined similarity index based on the Carbo index for electrostatics[43] and a shape similarity index to account for steric differences was evaluated (with both indices weighted equally) using three Gaussian functions for integration. This combined index was then optimized by overlaying the centroids of the molecules and performing a full translational and orientational search of each rigid comparison molecule relative to the lead compound pergolide (**21**) by systematically rotating around the Cartesian *x*-, *y*-, and *z*-axes in 10° steps. For each new orientation, a Simplex algorithm in combination with simulated annealing directs the six degrees of freedom to an alignment with optimal similarity.[41] Finally, the orientation and placement of each ligand on the template **21** with the highest score revealed by this search algorithm was chosen to yield the Tsar-based alignment (TBA). Although this alignment proved to be useful in first CoMFA approaches regarding the application of Advanced CoMFA H-bond fields, no significant regular CoMFA results involving steric and electrostatic interaction fields could be obtained ($q^2_{cv} = 0.36$; five components).

Thus, a rigid field fit (RFF) as implemented in Sybyl was performed for each molecule in its Tsar-based alignment on the steric and electrostatic CoMFA fields of **21**. It should be noted that, in contrast to the more frequently used flexible field fit, the carefully determined conformation of the ligands is completely maintained. As the field fit routine uses a gradient method to find the closest local optimum, only minor to moderate displacement of the ligands (rmsd 0.05−2.05 Å) could be observed. Albeit the full RFF-alignment only slightly improved the significance of the model ($q^2_{cv} = 0.44$; seven components), interestingly, detailed inspections revealed that some ligands seem to enhance the model quality, when being realigned with RFF, while others impair it.

Considering that systematic variation of 44 training set molecules in two alignment states requires more than 17.5×10^{12} calculations, we employed the self-written Spl[44] protocol IRAS (iterative restriction of alignment selection) to determine the favorable alignment state of each ligand. Within IRAS, mixed alignments are built by probability-based selection of an alignment state for each ligand and evaluated using their CoMFA model performance, calculated as the cross-validated q^2-value, as a fitness function. After taking 100 mixed alignment samples, the probability to select alignments with a superior performance is augmented for the subsequent sampling. Using this sequence of probability-based sampling, evaluation of the preferential alignment and adjustment of the probabilities was repeated in 15 iterations. Over the total number of 1500 evaluated mixed alignments, the range of model significance was enhanced successively to a $q^2_{cv} > 0.7$. A comparison of the investigator time between our approach and a more standard one involving "manual iterations" indicates that setting up one IRAS run takes a few hours and the run itself required about 1−2 days computation time for our test set on a regular single-processor workstation, whereas a manual systematic variation with $>10^{12}$ combinations is obviously not conceivable. A more detailed description of IRAS can be found in the Supporting Information. Thus, we obtained a superior IRAS-alignment, which we used for 3D-QSAR analyses, subsequently.

CoMFA and CoMSIA. The descriptive steric and electrostatic components of the CoMFA[27] intermolecular interaction field were calculated as implemented in SYBYL using Coulomb and Lennard-Jones potentials, respectively. A distance-dependent dielectric constant (1/*r*) was chosen, and the maximum field values were truncated to 30 kcal·mol^{-1} for the steric and ±50 kcal·mol^{-1} for the electrostatic interaction energies, applying a smooth transition to the cutoff plateau. The analysis was performed using a sp^3 carbon probe (C.3, charge +1.0) positioned at the lattice points (1 Å increment) of a regular grid. It was dimensioned to ensure that the distance of all atoms to the grid borders was at least 4 Å. Additionally, Böhm et al. attributed the dependence of the q^2_{cv} on the grid spacing and the positioning of the molecules within the lattice to the shape and steepness of the hyperbolic Lennard-Jones and Coulomb potentials.[25] As a consequence, increasing the lattice space also enhances the probability to lose important contributions to the PLS analysis, due to the required arbitrary fixation of the cutoff values. Thus, enlarging the increment to 1.5 or 2.0 Å impaired the quality of the model, as anticipated. To account for possible problems of the analysis arising from the absolute placement of the molecules within the grid space, it is useful to translate and/or rotate the entire data set within the lattice. Employing the APS (all placement search) script of Wang et al.,[26] the position of all molecules in the data set was systematically translated in steps of 0.1 Å in each direction along the *x*-, *y*-, and *z*-axis without changing their relative orientation. After each of 10^3 steps of translational displacement, the PLS analysis was repeated, giving a detailed insight into the positional dependence and robustness of the CoMFA.

The five physicochemical properties for CoMSIA[28] (steric, electrostatic, hydrophobic, and hydrogen-bond donor and acceptor) were evaluated using a common probe atom with 1 Å radius, +1.0 charge, and hydrophobicity and hydrogen-bond property values of + 1. The attenuation factor α, which determines the steepness of the Gaussian function, was assigned a default value of 0.3.[29] To allow for comparison between CoMFA and CoMSIA results, the APS-optimized grid box coordinates were used for the final models of both methods.

With the Partial Least Squares (PLS) technique, regression equations were obtained, explaining differences in the target properties (pK_i values) from differences in the interaction field data. To check the statistical significance of the models, cross-validations by the "leave-one-out" (LOO) method were performed. The optimal number of components was determined by the smallest predicted error sum of squares, s_{PRESS}. This value, which does not necessarily correspond to the highest q^2_{cv}, was used to derive the final QSAR model. In addition to the unfiltered data ($\sigma_{min} = 0.0$ kcal·mol^{-1}), further PLS

analyses were done considering only columns with a standard deviation of more than $\sigma_{min} = 1.0$ and 5.0 kcal·mol^{-1}, resulting in approximately 14% and 3.5% of the original data to be used, respectively. Although the field values in CoMSIA are not given by physical but by arbitrary units, a comparable column filtering effect was achieved by application of these σ_{min} values. It should be noted that, besides a substantial decrease in calculation time, noise reduction is the main reason for this column filtering. Another way to reduce the random, but cross-correlated, "brown noise" in the data matrix is region focusing,[45,46] a selective reweighting of the grid points in a region. Thus, we used the quite robust and generally recommended grid point-specific PLS parameter discriminant power with a default exponential factor of 0.3 in this procedure and obtained enhanced models, summarized with the previous ones in Table 3. The q^2, s_{PRESS}, r^2, and S values were calculated as defined in Sybyl.

Receptor Binding and Functional Assays. Dopamine receptor binding profiles were evaluated in comparison to the data of the reference compounds pramipexole and quinpirole (Table 2 and Supporting Information). D_1 and D_2 receptor binding utilizing native dopamine receptors was measured in competition experiments with bovine striatal membrane preparations employing the D_1 and D_2 selective radioligands [^{3}H]-SCH23390 and [^{3}H]spiperone, respectively.[47] The affinities to the human D_{2long}, D_{2short},[48] D_3,[49] and D_4[50] receptors were determined by utilizing membranes of Chinese hamster ovary cells stably expressing the different subtype of dopamine receptor and the radioligand [^{3}H]spiperone. Nonlinear regression analysis of the appropriate dose−response curves resulted in K_i values for antagonists or high and low K_i values for agonists. This differentiation was accomplished by calculation of the Hill slope and analyzing the best fit for a monophasic or a biphasic curve representing the binding of an antagonist to the low affinity binding site or of an agonist to the high- and low-affinity binding site of the receptor, respectively.

The most promising compounds, **(*S*)-9** and **(*S*)-10**, and the references pramipexole (**25**) and quinpirole (**27**) were further evaluated in a functional test measuring the stimulation of cell division induced by agonists (Table 2). This mitogenesis assay is based on the receptor-mediated stimulation of the incorporation of [^{3}H]thymidine into growing cells affording EC_{50} data and the amount of intrinsic activity relative to the reference quinpirole (=100%).[51]

(*S*)-7-Dipropylamino-5,6,7,8-tetrahydroindolizine-3-carbonitrile ((*S*)-10). To a solution of **(*S*)-9**[8] (58 mg, 0.234 mmol) in formic acid (1.5 mL) was added hydroxylamine hydrochloride (34 mg, 0.49 mmol) and the mixture was refluxed for 45 min. After cooling to room temperature, ice water (10 mL), 5 N NaOH, and diethyl ether were added. The organic layer was dried ($MgSO_4$) and evaporated and the residue was purified by flash chromatography (benzene/ethyl acetate 4:1) to give pure **(*S*)-10** (33 mg, 58%) as a colorless oil. $[\alpha]^{23}_D = -34.2°$ (*c* 0.8, $CHCl_3$). ^{1}H NMR ($CDCl_3$, 360 MHz): δ 0.88 (t, J = 7.4 Hz, 6H), 1.45 (sext, J = 7.4 Hz, 4H), 1.92 (dddd, J = 12.9, 12.3, 11.7, 5.5 Hz, 1H), 2.11−2.19 (m, 1H), 2.41−2.51 (m, 4H), 2.66 (dd, J = 16.1, 11.3 Hz, 1H), 2.95 (ddd, J = 16.1, 4.8, 1.7 Hz, 1H), 3.04 (dddd, J = 11.7, 11.3, 4.8, 2.8 Hz, 1H), 3.90 (ddd, J = 12.3, 12.3, 4.4 Hz, 1H), 4.30 (ddd, J = 12.3, 5.5, 2.4 Hz, 1H), 5.87 (d, J = 3.8 Hz, 1H), 6.75 (d, J = 3.8 Hz, 1H). EIMS (70 eV) *m/z*: 245 (M^+). Anal. ($C_{15}H_{23}N_3$): C, H, N. Starting from **(*R*)-9**, **(*R*)-10** [$[\alpha]^{23}_D$ = +32.9° (*c* 0.8, $CHCl_3$)] was prepared under the same reaction conditions.

(*S*)-1-(7-Dipropylamino-5,6,7,8-tetrahydroindolizin-3-yl)ethanone ((*S*)-11). To a suspension of $AlCl_3$ (61 mg, 0.46 mmol) in 1,2-dichloroethane (5 mL) was added acetyl chloride (33 μL, 0.45 mmol) at 0 °C. After 10 min, a solution of **(*S*)-1**[22] (20 mg, 0.09 mmol) in 1,2-dichloroethane (2 mL) was added and stirring was continued under reflux for 22 h. After being cooled to room temperature and addition of ice water and 2 N NaOH, the mixture was extracted with diethyl ether (30 mL) and the organic layer was dried ($MgSO_4$) and evaporated. The residue was purified by flash chromatography (petroleum ether/ethyl acetate 4:1 to petroleum ether/ethyl acetate 1:1) to give pure **(*S*)-11** (14 mg, 58%) as a colorless oil. $[\alpha]^{20}_D = -25.3°$ (*c* = 0.375). ^{1}H NMR ($CDCl_3$, 360 MHz): δ 0.88 (t, J = 7.3 Hz, 6H), 1.46 (sext, J = 7.3 Hz, 4H), 1.82 (dddd, J = 12.5, 12.5, 12.5, 5.7 Hz, 1H), 2.06−2.15 (m, 1H), 2.38 (s, 3H), 2.41−2.50 (m, 4H), 2.70 (dd, J = 16.6, 11.5 Hz, 1H), 2.91−3.07 (m, 2H), 4.02 (ddd, J = 12.5, 12.5, 4.6 Hz, 1H), 4.87 (ddd, J = 12.5, 5.7, 2.3 Hz, 1H), 5.90 (d, J = 4.1 Hz, 1H), 6.93 (d, J = 4.1 Hz, 1H). ^{13}C NMR ($CDCl_3$, 90 MHz): δ 11.81, 21.83, 26.56, 26.89, 27.12, 46.22, 52.41, 53.94, 106.76, 120.23, 129.54, 138.99, 187.46. EIMS *m/z*: 262. Anal. ($C_{16}H_{26}N_2O$): C, H, N. Starting from **(*R*)-1**, **(*R*)-11** [$[\alpha]^{20}_D$ = +26.4° (*c* 0.25)] was prepared under the same reaction conditions.

(*S*)-(7-Dipropylamino-5,6,7,8-tetrahydroindolizin-3-yl)-phenylmethanone ((*S*)-12). To a suspension of $AlCl_3$ (91 mg, 0.68 mmol) in 1,2-dichloroethane (8 mL) was added benzoyl chloride (76 μL, 0.68 mmol) at 0 °C. After 10 min, a solution of **(*S*)-1**[22] (30 mg, 0.14 mmol) in 1,2-dichloroethane (2 mL) was added and stirring was continued under reflux for 24 h. After being cooled to room temperature and addition of ice water and 2 N NaOH, the mixture was extracted with diethyl ether (30 mL) and the organic layer was dried ($MgSO_4$) and evaporated. The residue was purified by flash chromatography (dichloromethane/methanol 9:1) to give pure **(*S*)-12** (5 mg, 23%) as a yellow oil. $[\alpha]^{20}_D = -92.0°$ (*c* 0.25). ^{1}H NMR ($CDCl_3$, 360 MHz): δ 0.89 (t, J = 7.3 Hz, 6H), 1.48 (sext, J = 7.3 Hz, 4H), 1.89 (dddd, J = 12.3, 12.3, 11.4, 5.3 Hz, 1H), 2.12−2.22 (m, 1H), 2.42−2.56 (m, 4H), 2.77 (dd, J = 16.3, 11.0 Hz, 1H), 2.98−3.15 (m, 2H), 4.23 (ddd, J = 14.2, 11.4, 4.6 Hz, 1H), 4.94 (ddd, J = 14.2, 5.3, 2.5 Hz, 1H), 5.93 (d, J = 4.2 Hz, 1H), 6.71 (d, J = 4.2 Hz, 1H), 7.39−7.53 (m, 3H), 7.73−7.78 (m, 2H). EIMS *m/z*: 324. HRMS: *m/z* calcd for $C_{21}H_{28}N_2O$ 324.2202, found 324.2207. Starting from **(*R*)-1**, **(*R*)-12** [$[\alpha]^{20}_D$ = +94.6° (*c* 0.43)] was prepared under the same reaction conditions.

(*S*)-1-(7-Dipropylamino-5,6,7,8-tetrahydroindolizin-3-yl)-2,2,2-trifluorethanone ((*S*)-13). To a suspension of $AlCl_3$ (696 mg, 5.2 mmol) in dichloromethane (20 mL) was added trifluoroacidic acid anhydride (2.27 mL, 16.4 mmol) at 0 °C. After 20 min, a solution of **(*S*)-1**[22] (180 mg, 0.8 mmol) in dichloromethane (10 mL) was added and stirring was continued at room temperature for 3 h. After addition of ice water and 2 N NaOH, the mixture was extracted with dichloromethane (75 mL) and the organic layer was dried ($MgSO_4$) and evaporated. The residue was purified by flash chromatography (petroleum ether/ethyl acetate 4:1 to petroleum ether/ethyl acetate 1:1) to give pure **(*S*)-13** (193 mg, 75%) as a colorless oil. $[\alpha]^{20}_D = -26.4°$ (*c* 0.62). ^{1}H NMR ($CDCl_3$, 360 MHz): δ 0.89 (t, J = 7.3 Hz, 6H), 1.46 (sext, J = 7.3 Hz, 4H), 1.82 (dddd, J = 12.5, 12.5, 12.1, 5.6 Hz, 1H), 2.12−2.21 (m, 1H), 2.43−2.51 (m, 4H), 2.75 (dd, J = 17.1, 11.3 Hz, 1H), 2.96−3.12 (m, 2H), 4.08 (ddd, J = 14.2, 12.1, 4.1 Hz, 1H), 4.83 (ddd, J = 14.2, 5.6, 2.4 Hz, 1H), 6.05 (d, J = 4.5 Hz, 1H), 7.17−7.21 (m, 1H). ^{13}C NMR ($CDCl_3$, 63 MHz): δ 11.77, 21.62, 26.19, 27.39, 46.47, 52.35, 53.43, 109.58, 119.67, 123.61, 124.30, 124.37, 144.01. EIMS *m/z*: 316. Anal. ($C_{16}H_{23}F_3N_2O$): C, H, N. Starting from **(*R*)-1**, **(*R*)-13** [$[\alpha]^{20}_D$ = +27.2° (*c* = 0.95)] was prepared under the same reaction conditions.

(*S*)-1-(7-Dipropylamino-5,6,7,8-tetrahydroindolizin-3-yl)-2,2,2-trichlorethanone ((*S*)-14). To a suspension of trichloracetyl chloride (75μL, 0.68 mmol) in diethyl ether (5 mL) was added a solution of **(*S*)-1**[22] (50 mg, 0.234 mmol) in diethyl ether (10 mL) and stirring was continued under reflux for 6 h. After addition of a saturated Na_2CO_3, the mixture was extracted with diethyl ether (30 mL) and the organic layer was dried ($MgSO_4$) and evaporated. The residue was purified by flash chromatography (petroleum ether/ethyl acetate 95:5, petroleum ether/ethyl acetate 4:1) to give pure **(*R*)-14** (62 mg, 75%) as a colorless oil. $[\alpha]^{20}_D = -21.1°$ (*c* 0.63). ^{1}H NMR ($CDCl_3$, 360 MHz): δ 0.89 (t, J = 7.3 Hz, 6H), 1.46 (sext, J = 7.3 Hz, 4H), 1.87 (dddd, J = 12.2, 12.2, 12.1, 5.6 Hz, 1H), 2.12−2.21 (m, 1H), 2.42−2.52 (m, 4H), 2.75 (dd, J = 17.0, 11.4 Hz, 1H), 2.96−3.12 (m, 2H), 4.09 (ddd, J = 14.2, 12.2, 5.0 Hz, 1H), 4.83 (ddd, J = 14.2, 5.6, 2.2 Hz, 1H), 6.02 (d, J = 4.4 Hz, 1H), 7.50 (d, J = 4.4 Hz, 1H). EIMS *m/z*: 364, 366, 368, 370. Anal.

($C_{16}H_{23}N_2OCl_3$): C, H, N. Starting from **(*R*)-1**, **(*R*)-14** [$[\alpha]^{20}_D$ = +21.9° (*c* 0.21)] was prepared under the same reaction conditions.

(*S*)-7-Dipropylamino-5,6,7,8-tetrahydroindolizine-3-carboxylic Acid Ethyl Ester ((*S*)-15). After reaction of sodium (1.2 mg, 0.05 mmol) in ethanol (1 mL), a solution of **(*S*)-14** (62 mg, 0.17 mmol) in ethanol (9 mL) was added. After being refluxed for 18 h, the reaction mixture was cooled to room temperature. Then, saturated $NaHCO_3$ and diethyl ether (30 mL) were added. The organic layer was dried ($MgSO_4$) and evaporated and the residue was purified by flash chromatography (petroleum ether/ethyl acetate 4:1) to give **(*S*)-15** (28 mg, 65%) as a colorless oil. $[\alpha]^{20}_D$ = −19.9° (*c* 0.29). ^{1}H NMR ($CDCl_3$, 360 MHz): δ 0.88 (t, *J* = 7.4 Hz, 6H), 1.32 (t, *J* = 7.2 Hz, 3H), 1.46 (sext, *J* = 7.4 Hz, 4H), 1.86 (dddd, *J* = 12.4, 12.4, 12.0, 5.5 Hz, 1H), 2.07−2.16 (m, 1H), 2.42−2.50 (m, 4H), 2.69 (dd, *J* = 16.3, 11.5 Hz, 1H), 2.96−3.06 (m, 2H), 3.98 (ddd, *J* = 13.7, 12.4, 4.8 Hz, 1H), 4.24 (q, *J* = 7.2 Hz, 2H), 4.82 (ddd, *J* = 13.7, 5.5, 2.4 Hz, 1H), 5.87 (d, *J* = 4.1 Hz, 1H), 6.92 (d, *J* = 4.1 Hz, 1H). EIMS *m/z*: 292. Anal. ($C_{17}H_{28}N_2O_2$): C, H, N. Starting from **(*R*)-14**, **(*R*)-15** [$[\alpha]^{20}_D$ = +18.9° (*c* 0.28)] was prepared under the same reaction conditions.

***E*-(*S*)-7-Dipropylamino-5,6,7,8-tetrahydoindolizine-3-carbaldehyde Oxime ((*S*)-16) and *Z*-(*S*)-7-Dipropylamino-5,6,7,8-tetrahydoindolizine-3-carbaldehyde Oxime ((*S*)-17).** To a solution of hydroxylamine hydrochloride (13 mg, 0.36 mmol) in water (2 mL) was added 2 N NaOH (90 μL, 0.18 mmol) at 0 °C. The mixture was adjusted to pH 5 by 2 N HCl. After addition of **(*S*)-9**[8] (45 mg, 0.18 mmol) in ethanol (9 mL), the mixture was refluxed for 2 h. Then, the mixture was concentrated to 50% of the volume, and saturated $NaHCO_3$ and diethyl ether (30 mL) were added. The organic layer was dried ($MgSO_4$) and evaporated and the residue was purified by flash chromatography (dichloromethane/methanol 98:2 to dichloromethane/methanol 95:5) to give pure **(*S*)-16** (21 mg, 55%) as a colorless solid (mp 104−108 °C) and, subsequently, pure **(*S*)-17** (11 mg, 29%) as a colorless solid (mp 138 °C). Analytical data **(*S*)-16**: $[\alpha]^{23}_D$ = −13.9° (*c* 0.29). ^{1}H NMR ($CDCl_3$, 360 MHz): δ 0. 89 (t, *J* = 7.3 Hz, 6H), 1.48 (sext, *J* = 7.3 Hz, 4H), 1.90 (dddd, *J* = 12.3, 12.3, 12.0, 5.5 Hz, 1H), 2.15−2.25 (m, 1H), 2.38−2.56 (m, 4H), 2.70 (dd, *J* = 15.6, 11.4 Hz, 1H), 2.93−3.12 (m, 2H), 3.90 (ddd, *J* = 13.1, 12.3, 4.6 Hz, 1H), 4.54 (ddd, *J* = 13.1, 5.5, 2.1 Hz, 1H), 5.89 (d, *J* = 3.5 Hz, 1H), 6.34 (d, *J* = 3.5 Hz, 1H), 8.00 (s, 1H). HPLC: t_R = 8.75 min (Eurospher RP-18, aqueous NH_4Cl solution (1%)/ethanol 4:1, UV: 290 nm). UV (MeOH): λ_{max} (nm) [log ϵ]: 289 [4.04]. EIMS *m/z*: 263. Anal. ($C_{15}H_{25}N_3O$): C, H, N. Starting from **(*R*)-9**, **(*R*)-16** [$[\alpha]^{20}_D$ = +15.3° (*c* 0.55)] was prepared under the same reaction conditions**.** Analytical data **(*S*)-17**: $[\alpha]^{20}_D$ = −34.4° (*c* 0.22). ^{1}H NMR ($CDCl_3$, 360 MHz): δ 0. 89 (t, *J* = 7.3 Hz, 6H), 1.46 (sext, *J* = 7.3 Hz, 4H), 1.90 (dddd, *J* = 12.4, 12.4, 11.3, 5.7 Hz, 1H), 2.12−2.21 (m, 1H), 2.43−2.52 (m, 4H), 2.70 (dd, *J* = 16.0, 11.4 Hz, 1H), 2.94−3.07 (m, 2H), 3.88 (ddd, *J* = 12.1, 11.3, 4.6 Hz, 1H), 4.28 (ddd, *J* = 12.1, 5.7, 2.5 Hz, 1H), 5.99 (d, *J* = 3.7 Hz, 1H), 7.24 (d, *J* = 3.7 Hz, 1H), 7.36 (s, 1H). HPLC: t_R = 6.75 min (conditions as for **(*S*)-16**). UV (MeOH): λ_{max} (nm) [log ϵ]: 293 [4.28]. HRMS: *m/z* calcd for $C_{15}H_{25}N_3O$ 263.1998, found 263.1989. Starting from **(*R*)-9**, **(*R*)-17** [$[\alpha]^{20}_D$ = +35.4° (*c* 0.35)] was prepared under the same reaction conditions.

(*S*)-7-Dipropylamino-3-phenyl-5,6,7,8-tetrahydroindolizine ((*S*)-28). To a solution of *(S)*-4-amino-2-dibenzylamino-butanol[22] (1.6 g, 2.1 mmol) and sodium acetate (5.2 g, 63 mmol) in acidic acid (30 mL) was added a solution of 4-oxo-4-phenylbutyraldehyde[52] (0.6 g, 3.7 mmol) in acidic acid (25 mL) at room temperature. The solution was heated at 70 °C for 75 min. After evaporation, 2 N NaOH and diethyl ether were added at 0 °C. The organic layer was evaporated and the residue was treated with a mixture of methanol (40 mL) and K_2CO_3 (1.5 g) dissolved in water (20 mL). After being stirred for 24 h at room temperature, the mixture was concentrated and extracted with diethyl ether. The organic layer was dried ($MgSO_4$) and evaporated and the residue was purified by flash chromatography (benzene/ethyl acetate 4:1) to give (*S*)-2-dibenzylamino-4-(2-phenylpyrrol-1-yl)butan-1-ol (intermediate I) (1.21 g, 80%) as a yellowish oil. $[\alpha]^{23}_D$ = +62.2° (*c* 1.0, $CHCl_3$). ^{1}H NMR ($CDCl_3$, 360 MHz): δ 1.42−1.54 (m, 1H), 1.92−2.04 (m, 1H), 2.60−2.75 (m, 2H), 3.21 (d, *J* = 13.2 Hz, 2H), 3.22 (dd, *J* = 10.1, 5.5 Hz, 1H), 3.36 (dd, *J* = 10.1, 10.1 Hz, 1H), 3.65 (d, *J* = 13.2 Hz, 2H), 3.81−4.02 (m, 2H), 6.20 (dd, *J* = 3.4, 1.7 Hz, 1H), 6.22 (dd, *J* = 3.4, 2.9 Hz, 1H), 6.70 (dd, *J* = 2.9, 1.7 Hz, 1H), 7.09−7.15 (m, 4H), 7.19−7.43 (m, 11H). CIMS (methane) *m/z*: 411 (M + 1). Anal. ($C_{28}H_{30}N_2O$): C, H, N. To a solution of the intermediate I (1.1 g, 2.68 mmol) in dichloromethane (50 mL) was added triethylamine (360 mg, 3.56 mmol) and trifluoromethanesulfonic anhydride (873 mg, 3.09 mmol) at 0 °C. The solution was stirred at room temperature for 24 h when another portion of triethylamine (360 mg, 3.56 mmol) and trifluoromethanesulfonic anhydride (873 mg, 3.09 mmol) was added at room temperature. After 1 h, saturated $NaHCO_3$ and diethyl ether were added. The organic layer was dried ($MgSO_4$) and evaporated and the residue was purified by flash chromatography (benzene/diethyl ether 95:5) to give pure (*S*)-7-dibenzylamino-3-phenyl-5,6,7,8-tetrahydroindolizine (intermediate II) as a colorless solid (545 mg, 52%). Mp: 46−48 °C. $[\alpha]^{23}_D$ = +71.5° (*c* 0.4, $CHCl_3$). ^{1}H NMR ($CDCl_3$, 360 MHz): δ 1.92 (dddd, *J* = 12.1, 12.1, 12.1, 5.1 Hz, 1H), 2.10−2.20 (m, 1H), 2.96 (dd, *J* = 14.9, 11.1 Hz, 1H), 3.06−3.22 (m, 2H), 3.67 (d, *J* = 13.7 Hz, 2H), 3.71−3.81 (m, 1H), 3.75 (d, *J* = 13.7 Hz, 2H), 4.13 (ddd, *J* = 12.2, 5.0, 2.3 Hz, 1H), 5.93 (d, *J* = 3.4 Hz, 1H), 6.17 (d, *J* = 3.4 Hz, 1H), 7.15−7.43 (m, 15H). EIMS (70 eV) *m/z*: 392 (M^+). Anal. ($C_{28}H_{28}N_2$): C, H, N. Intermediate II (337 mg, 0.86 mmol) and 20% $Pd(OH)_2$/C (350 mg) in ethyl acetate (30 mL) and methanol (30 mL) were stirred at room temperature for 24 h under a balloon of hydrogen. After filtration through Celite, the mixture was evaporated and the residue was purified by flash chromatography (dichloromethane/methanol 4:1) to give pure (*S*)-7-amino-3-phenyl-5,6,7,8-tetrahydroindolizine (intermediate III) (143 mg, 79%) as a colorless solid. Mp: 170 °C (dec). $[\alpha]^{23}_D$ = −10.0° (*c* 0.1, MeOH/$CHCl_3$ 1:1). ^{1}H NMR (CD_3OD/$CDCl_3$ 1:1, 360 MHz): δ 1.88 (dddd, *J* = 13.0, 10.7, 10.3, 5.2 Hz, 1H), 2.14−2.25 (m, 1H), 2.70 (ddd, *J* = 15.6, 9.9, 0.3 Hz, 1H), 3.21 (ddd, *J* = 15.6, 5.1, 0.9 Hz, 1H), 3.35 (dddd, *J* = 10.3, 9.9, 5.1, 3.5 Hz, 1H), 3.92 (ddd, *J* = 12.7, 10.7, 4.6 Hz, 1H), 4.14 (ddd, *J* = 12.7, 5.2, 4.1 Hz, 1H), 5.94 (br.d, *J* = 3.4 Hz, 1H), 6.17 (d, *J* = 3.4 Hz, 1H), 7.24−7.31 (m, 1H), 7.34−7.41 (m, 4H). EIMS (70 eV) *m/z*: 212 (M^+). Anal. ($C_{14}H_{16}N_2$): C, H, N. To a solution of intermediate III (55 mg, 0.26 mmol) in methanol (25 mL) were added propionic aldehyde (150 mg, 2.58 mmol) and sodium cyanoborohydride (32 mg, 0.51 mmol) at 0 °C. The solution was stirred at 0 °C for 15 min and subsequently at room temperature for 18 h and then acidified with 2 N HCl and finally basified with saturated $NaHCO_3$. After addition of diethyl ether, the organic layer was dried ($MgSO_4$) and evaporated and the residue was purified by flash chromatography (benzene/ethyl acetate 4:1) to give pure **(*S*)-28** (53 mg, 69%) as a colorless oil. $[\alpha]^{23}_D$ = +32.2° (*c* 1.0, $CHCl_3$). ^{1}H NMR ($CDCl_3$, 360 MHz): δ 0.89 (t, *J* = 7.4 Hz, 6H), 1.47 (sext, *J* = 7.4 Hz, 4H), 1.84 (dddd, *J* = 12.2, 12.2, 12.2, 5.0 Hz, 1H), 2.02−2.11 (m, 1H), 2.41−2.53 (m, 4H), 2.78 (br.dd, *J* = 14.9, 10.4 Hz, 1H), 3.00−3.15 (m, 2H), 3.87 (ddd, *J* = 12.2, 12.2, 4.2 Hz, 1H), 4.16 (ddd, *J* = 12.2, 5.0, 2.5 Hz, 1H), 5.94 (br.d, *J* = 3.4 Hz, 1H), 6.20 (d, *J* = 3.4 Hz, 1H), 7.22−7.28 (m, 1H), 7.33−7.40 (m, 4H). EIMS (70 eV) *m/z*: 296 (M^+). HRMS: *m/z* calcd for $C_{20}H_{28}N_2$: 296.2252, found 296.2263 (M^+). **(*R*)-28** [$[\alpha]^{23}_D$ = −33.3° (*c* 0.1, $CHCl_3$)] was prepared under the same reaction conditions.

(*S*)-2-(7-Dipropylamino-5,6,7,8-tetrahydroindolizin-3-ylmethylene)malonitrile ((*S*)-29). To a suspension of **(*S*)-9**[8] (50 mg, 0.20 mmol) and malononitrile (23 mg, 0.35 mmol) in 70% methanol (1.4 mL) was added piperidine (37 μL, 32 mg, 0.38 mmol). After being stirred at room temperature for 90 min, the mixture was concentrated and the residue was purified by flash chromatography (benzene/ethyl acetate 4:1) to give pure **(*S*)-29** (41 mg, 69%) as a yellow solid. Mp: 110−111 °C. $[\alpha]^{23}_D$ = −57.7° (*c* 1.0, $CHCl_3$). ^{1}H NMR ($CDCl_3$, 360 MHz): δ 0.89 (t, *J* = 7.4 Hz, 6H), 1.45 (sext, *J* = 7.4 Hz, 4H),

1.94 (dddd, J = 12.9, 11.9, 11.9, 5.4 Hz, 1H), 2.16−2.27 (m, 1H), 2.39−2.54 (m, 4H), 2.77 (dd, J = 17.5, 10.8 Hz, 1H), 2.96−3.12 (m, 2H), 3.85 (ddd, J = 12.1, 11.9, 4.8 Hz, 1H), 4.24 (ddd, J = 12.1, 5.5, 2.7 Hz, 1H), 6.20 (d, J = 4.6 Hz, 1H), 7.39 (s, 1H), 7.65 (d, J = 4.6 Hz, 1H). EIMS (70 eV) *m/z*: 296 (M^+). Anal. ($C_{18}H_{24}N_4$): C, H, N. Starting from **(*R*)-9**, **(*R*)-29** [$[\alpha]^{23}_D$ = +59.0° (*c* 0.4, $CHCl_3$)] was prepared under the same reaction conditions.

(*S*)-3-Dimethylaminomethyl-7-*N*,*N*-dipropylamino-5,6,7,8-tetrahydroindolizine ((*S*)-30). To a solution of **(*S*)-9**[8] (32 mg, 0.129 mmol) in methanol (5 mL) were added dimethylammonium chloride (53 mg, 0.65 mmol) and sodium cyanoborohydride (16 mg, 0.25 mmol) at 0 °C. After being stirred at room temperature for 24 h, further portions of dimethylammonium chloride (53 mg, 0.65 mmol) and sodium cyanoborohydride (16 mg, 0.25 mmol) were added, and stirring was continued for further 24 h at room temperature. After evaporation, saturated $NaHCO_3$ and diethyl ether were added. The organic layer was dried ($MgSO_4$) and evaporated and the residue was purified by flash chromatography (dichloromethane/methanol 4:1) to give pure **(*S*)-30** (23 mg, 64%) as a colorless oil besides starting material (9 mg). ^{1}H NMR ($CDCl_3$, 360 MHz): δ 0.87 (t, J = 7.4 Hz, 6H), 1.45 (sext, J = 7.4 Hz, 4H), 1.86 (dddd, J = 12.3, 12.3, 12.1, 5.4 Hz, 1H), 2.02−2.11 (m, 1H), 2.18 (s, 6H), 2.39−2.52 (m, 4H), 2.66 (br.dd, J = 14.8, 11.3 Hz, 1H), 2.89−3.05 (m, 2H), 3.25 (d, J = 13.4 Hz, 1H), 3.32 (d, J = 13.4 Hz, 1H), 3.73 (ddd, J = 12.4, 12.3, 4.8 Hz, 1H), 4.25 (ddd, J = 12.4, 5.4, 2.3 Hz, 1H), 5.75 (br.d, J = 3.1 Hz, 1H), 5.94 (d, J = 3.1 Hz, 1H). EIMS (70 eV) *m/z*: 277 (M^+). Anal. ($C_{17}H_{31}N_3$): C, H, N. Starting from **(*R*)-9**, **(*R*)-30** was prepared under the same reaction conditions.

Acknowledgment. The authors wish to thank Dr. H. H. M. Van Tol (Clarke Institute of Psychiatry, Toronto) and Dr. J. -C. Schwartz and Dr. P. Sokoloff (INSERM, Paris) as well as J. Shine (The Garvan Institute of Medical Research, Sydney) for providing dopamine D_4, D_3, and D_2 receptor expressing cell lines, respectively. This work was supported by the BMBF and Fonds der Chemischen Industrie.

Supporting Information Available: Full experimental section, dopamine receptor binding profiles of **9**−**17** and **28**−**31**, and an overview plus a detailed explanation of the newly invented Spl application IRAS (the corresponding Spl script can be obtained on request from the authors). This material is available free of charge via the Internet at http://pubs.acs.org.

References

(1) Sokoloff, P.; Giros, B.; Martres, M. P.; Bouthenet, M. L.; Schwartz, J. C. Molecular cloning and characterization of a novel dopamine receptor (D3) as a target for neuroleptics. *Nature* **1990**, *347*, 146−151.
(2) Neve, K. A.; Neve, R. L. *The dopamine receptors*; Humana Press: Totowa, NJ, 1997.
(3) Richtand, N. M.; Woods, S. C.; Berger, S. P.; Strakowski, S. M. D3 dopamine receptor, behavioral sensitization, and psychosis. *Neurosci. Biobehav. Rev.* **2001**, *25*, 427−443.
(4) Joyce, J. N.; Ryoo, H. L.; Beach, T. B.; Caviness, J. N.; Stacy, M.; Gurevich, E. V.; Reiser, M.; Adler, C. H. Loss of response to levodopa in Parkinson's disease and co-occurrence with dementia: Role of D3 and not D2 receptors. *Brain Res.* **2002**, *955*, 138−152.
(5) Bezard, E.; Ferry, S.; Mach, U.; Stark, H.; Leriche, L.; Boraud, T.; Gross, C.; Sokoloff, P. Attenuation of levodopa-induced dyskinesia by normalizing dopamine D3 receptor function. *Nat. Med.* **2003**, *9*, 762−767.
(6) Pilla, M.; Perachon, S.; Sautel, F.; Garrido, F.; Mann, A.; Wermuth, C. G.; Schwartz, J. C.; Everitt, B. J.; Sokoloff, P. Selective inhibition of cocaine-seeking behaviour by a partial dopamine D3 receptor agonist. *Nature* **1999**, *400*, 371−375.
(7) Unis, A. S.; Roberson, M. D.; Hill, K.; Hamblin, M. W.; Dorsa, D. W. Differential localization of D2 versus D3 mRNA in midgestational human forebrain by in situ hybridization. *Soc. Neurosc. Abstr.* **1995**, 1620.
(8) Lehmann, T.; Hübner, H.; Gmeiner, P. Dopaminergic 7-aminotetrahydroindolizines: Ex-chiral pool synthesis and preferential D3 receptor binding. *Bioorg. Med. Chem. Lett.* **2001**, *11*, 2863−2866.
(9) Brusniak, M. Y.; Pearlman, R. S.; Neve, K. A.; Wilcox, R. E. Comparative molecular field analysis-based prediction of drug affinities at recombinant D1A dopamine receptors. *J. Med. Chem.* **1996**, *39*, 850−859.
(10) Wilcox, R. E.; Tseng, T.; Brusniak, M. Y.; Ginsburg, B.; Pearlman, R. S.; Teeter, M.; DuRand, C.; Starr, S.; Neve, K. A. CoMFA-based prediction of agonist affinities at recombinant D1 vs D2 dopamine receptors. *J. Med. Chem.* **1998**, *41*, 4385−4399.
(11) Wilcox, R. E.; Huang, W. H.; Brusniak, M. Y.; Wilcox, D. M.; Pearlman, R. S.; Teeter, M. M.; DuRand, C. J.; Wiens, B. L.; Neve, K. A. CoMFA-based prediction of agonist affinities at recombinant wild type versus serine to alanine point mutated D2 dopamine receptors. *J. Med. Chem.* **2000**, *43*, 3005−3019.
(12) Ravina, E.; Negreira, J.; Cid, J.; Masaguer, C. F.; Rosa, E.; Rivas, M. E.; Fontenla, J. A.; Loza, M. I.; Tristan, H.; Cadavid, M. I.; Sanz, F.; Lozoya, E.; Carotti, A.; Carrieri, A. Conformationally constrained butyrophenones with mixed dopaminergic (D(2)) and serotoninergic (5-HT(2A), 5-HT(2C)) affinities: Synthesis, pharmacology, 3D-QSAR, and molecular modeling of (aminoalkyl)-benzo- and -thienocycloalkanones as putative atypical antipsychotics. *J. Med. Chem.* **1999**, *42*, 2774−2797.
(13) Norinder, U.; Hogberg, T. A quantitative structure−activity relationship for some dopamine D2 antagonists of benzamide type. *Acta Pharm. Nord.* **1992**, *4*, 73−78.
(14) McGaughey, G. B.; Mewshaw, R. E. Application of comparative molecular field analysis to dopamine D2 partial agonists. *Bioorg. Med. Chem.* **1999**, *7*, 2453−2456.
(15) Homan, E. J.; Tulp, M. T.; Nilsson, J. E.; Wikstrom, H. V.; Grol, C. J. C5-substituted derivatives of 5-OMe-BPAT: Synthesis and interactions with dopamine D2 and serotonin 5-HT1A receptors. *Bioorg. Med. Chem.* **1999**, *7*, 2541−2548.
(16) Hackling, A.; Ghosh, R.; Perachon, S.; Mann, A.; Holtje, H. D.; Wermuth, C. G.; Schwartz, J. C.; Sippl, W.; Sokoloff, P.; Stark, H. N−(omega-(4-(2-methoxyphenyl)piperazin-1-yl)alkyl)carboxamides as dopamine D2 and D3 receptor ligands. *J. Med. Chem.* **2003**, *46*, 3883−3899.
(17) De Paulis, T.; El Tayar, N.; Carrupt, P. A.; Testa, B.; Van de Waterbeemd, H. Quantitative structure-affinity relationships of dopamine D2 receptor antagonists: A comparison between orthopramides and 6-methoxysalicylamides. *Helv. Chim. Acta* **1991**, *74*, 241−254.
(18) Cha, M. Y.; Lee, I. Y.; Cha, J. H.; Choi, K. I.; Cho, Y. S.; Koh, H. Y.; Pae, A. N. QSAR studies on piperazinylalkylisoxazole analogues selectively acting on dopamine D3 receptor by HQSAR and CoMFA. *Bioorg. Med. Chem.* **2003**, *11*, 1293−1298.
(19) Bostrom, J.; Gundertofte, K.; Liljeforsa, T. A pharmacophore model for dopamine D4 receptor antagonists. *J. Comput. Aided Mol. Des.* **2000**, *14*, 769−786.
(20) Bostrom, J.; Bohm, M.; Gundertofte, K.; Klebe, G. A 3D QSAR study on a set of dopamine D4 receptor antagonists. *J. Chem. Inf. Comput. Sci.* **2003**, *43*, 1020−1027.
(21) Lanig, H.; Utz, W.; Gmeiner, P. Comparative molecular field analysis of dopamine D4 receptor antagonists including 3-[4-(4-chlorophenyl)piperazin-1-ylmethyl]pyrazolo[1,5-*a*]pyridine (FAUC 113), 3-[4-(4-chlorophenyl)piperazin-1-ylmethyl]-1*H*-pyrrolo-[2,3-*b*]pyridine (L-745,870), and clozapine. *J. Med. Chem.* **2001**, *44*, 1151−1157.
(22) Gmeiner, P.; Lerche, H. New and efficient synthesis of 5,6,7,8-tetrahydroindolizidines. Application to the synthesis of pharmacologically relevant chiral aminoderivatives from L-asparagine. *Heterocycles* **1990**, *31*, 9−12.
(23) In contrast to CoMFA fields, CoMSIA similarity indices fields are not defined in physical but in arbitrary units.
(24) Thibaut, U.; Folkers, G.; Klebe, G.; Kubinyi, H.; Merz, A.; Rognan, D. Recommendations to CoMFA Studies and 3D QSAR Publications. In *3D QSAR in Drug Design. Theory, Methods and Applications*; Kubinyi, H., Ed.; ESCOM: Leiden, The Netherlands, 1993; pp 711−716.
(25) Böhm, M.; Stürzebecher, J.; Klebe, G. Three-dimensional quantitative structure−activity relationship analyses using comparative molecular field analysis and comparative molecular similarity indices analysis to elucidate selectivity differences of inhibitors binding to trypsin, thrombin, and factor Xa. *J. Med. Chem.* **1999**, *42*, 458−477.
(26) Wang, R.; Gao, Y.; Liu, L.; Lai, L. All-orientation search and all-placement search in comparative molecular field analysis. *J. Mol. Model.* **1998**, *4*, 276−283.
(27) Cramer, R. D., III; Patterson, D. E.; Bunce, J. D. Comparative molecular field analysis (CoMFA). 1. Effect of shape on binding of steroids to carrier proteins. *J. Am. Chem. Soc.* **1988**, *110*, 5959−5967.

(28) Klebe, G.; Abraham, U.; Mietzner, T. Molecular similarity indices in a comparative analysis (CoMSIA) of drug molecules to correlate and predict their biological activity. *J. Med. Chem.* **1994**, *37*, 4130−4146.
(29) Klebe, G.; Abraham, U. Comparative molecular similarity index analysis (CoMSIA) to study hydrogen-bonding properties and to score combinatorial libraries. *J. Comput. Aided Mol. Des.* **1999**, *13*, 1−10.
(30) Gohlke, H.; Schwarz, S.; Gundisch, D.; Tilotta, M. C.; Weber, A.; Wegge, T.; Seitz, G. 3D QSAR analyses-guided rational design of novel ligands for the (alpha4)2(beta2)3 nicotinic acetylcholine receptor. *J. Med. Chem.* **2003**, *46*, 2031−2048.
(31) Oliveira, L.; Hulsen, T.; Lutje Hulsik, D.; Paiva, A. C. M.; Vriend, G. Heavier-than-air flying machines are impossible. *FEBS Lett.* **2004**, *564*, 269−273.
(32) Boeckler, F.; Lanig, H.; Gmeiner, P. Modeling the similarity and divergence of dopamine D2-like receptors and identification of validated ligand−receptor complexes. *J. Med. Chem.* **2005**,*48*, 694−709.
(33) SYBYL 6.9, Tripos Inc., 1699 South Hanley Road, St. Louis, MO 63144.
(34) *TSAR V3.2*; Oxford Molecular Ltd., The Medawar Centre, Oxford Science Park, Sandford-on-Thames, Oxford OX4 4GA, U.K.
(35) Clark, M.; Cramer, R.-D.; Van Opdenbosch, N. Validation of the general purpose Tripos 5.2 force field. *J. Comput. Chem.* **1989**, *10*, 982−1012.
(36) Gasteiger, J.; Marsili, M. Iterative partial equalization of orbital electronegativity: A rapid access to atomic charges. *Tetrahedron* **1980**, *36*, 3219−3222.
(37) Clark, T.; Alex, A.; Beck, B.; Chandrasekar, J.; Gedeck, P.; Horn, A.; Huttern, M.; Martin, B.; Rauhut, G.; Sauer, W.; Schindler, T.; Steinke, T. *VAMP 7.0 Program Package*; Oxford Molecular Plc.: Oxford, 1998.
(38) Homan, E. J.; Wikstrom, H. V.; Grol, C. J. Molecular modeling of the dopamine D2 and serotonin 5-HT1A receptor binding modes of the enantiomers of 5-OMe-BPAT. *Bioorg. Med. Chem.* **1999**, *7*, 1805−1820.
(39) Gaedt, K. Theoretische Untersuchungen zur Bindungsstelle von Dopamin-D3-Rezeptor-Agonisten. PhD-thesis, Mathematisch-Naturwissenschaftliche Fakultät, Heinrich-Heine Universität, Düsseldorf, 1998; p 232.
(40) Ballesteros, J.; Weinstein, H. Integrated methods for the construction of three-dimensional models of structure−function relations in G protein-coupled receptors. In *Methods in Neurosciences: Receptor Molecular Biology*; Sealfon, S. C., Conn, M. P., Eds.; Academic Press: San Diego, CA, 1995; pp 366−428.
(41) *ASP V3.22*; Oxford Molecular Ltd., The Medawar Centre, Oxford Science Park, Sandford-on-Thames, Oxford OX4 4GA, U.K.
(42) Beck, B.; Clark, T.; Glen, R. C. A detailed study of VESPA electrostatic potential-derived atomic charges. *J. Mol. Model.* **1995**, *1*, 176−187.
(43) Carbo, R.; Leyda, L.; Arnau, M. How similar is a molecule to another? An electron density measure of similarity between two molecular structures. *Int. J. Quantum Chem.* **1980**, *17*, 1185−1189.
(44) Sybyl Programming Language.
(45) Lindgren, F.; Geladi, P.; Rännar, S.; Wold, S. Interactive variable selection (IVS) for PLS. Part 1: Theory and algorithms. *J. Chemometr.* **1994**, *8*, 349−363.
(46) Forina, M.; Casolino, C.; Pizarro Millan, C. Iterative predictor weighting (IPW) PLS: A technique for the elimination of useless predictors in regression problems. *J. Chemometr.* **1999**, *13*, 165−184.
(47) Hübner, H.; Haubmann, C.; Utz, W.; Gmeiner, P. Conjugated enynes as nonaromatic catechol bioisosteres: Synthesis, binding experiments, and computational studies of novel dopamine receptor agonists recognizing preferentially the D(3) subtype. *J. Med. Chem.* **2000**, *43*, 756−762.
(48) Hayes, G.; Biden, T. J.; Selbie, L. A.; Shine, J. Structural subtypes of the dopamine D2 receptor are functionally distinct: Expression of the cloned D2A and D2B subtypes in a heterologous cell line. *Mol. Endocrinol.* **1992**, *6*, 920−926.
(49) Sokoloff, P.; Andrieux, M.; Besancon, R.; Pilon, C.; Martres, M. P.; Giros, B.; Schwartz, J. C. Pharmacology of human dopamine D3 receptor expressed in a mammalian cell line: Comparison with D2 receptor. *Eur. J. Pharmacol.* **1992**, *225*, 331−337.
(50) Asghari, V.; Sanyal, S.; Buchwaldt, S.; Paterson, A.; Jovanovic, V.; Van Tol, H. H. Modulation of intracellular cyclic AMP levels by different human dopamine D4 receptor variants. *J. Neurochem.* **1995**, *65*, 1157−1165.
(51) Hübner, H.; Kraxner, J.; Gmeiner, P. Cyanoindole derivatives as highly selective dopamine D(4) receptor partial agonists: Solid-phase synthesis, binding assays, and functional experiments. *J. Med. Chem.* **2000**, *43*, 4563−4569.
(52) Severin, T.; Adam, R.; Lerche, H. *Chem. Ber.* **1975**, *108*, 1756.
(53) Bergauer, M.; Hübner, H.; Gmeiner, P. Practical ex-chiral-pool methodology for the synthesis of dopaminergic tetrahydroindoles. *Tetrahedron* **2004**, *60*, 1197−1204.
(54) Bush, B. L.; Nachbar, R. B., Jr. Sample-distance partial least squares: PLS optimized for many variables, with application to CoMFA. *J. Comput. Aided Mol. Des.* **1993**, *7*, 587−619.
(55) A contribution level of x% means that the xth percentile of the field values is contoured.

JM049269+